Feb. 7, 2017.

Atmos. Chem. Phys.

RE: Manuscript Number: acp-2016-732

Dear Editors:

Thank you very much for your kind decision letter on our paper entitled "**Improving $PM_{2.5}$ forecast over China by the joint adjustment of initial conditions and source emissions with an ensemble Kalman**" (acp-2016-732). We are grateful for the helpful comments from you and the reviewers. We have changed the manuscript according to the reviewer's suggestions. We hope this manuscript will be published in ACP. We are looking forward to hearing from you soon.

Sincerely Yours,

Zhen Peng

Response to Reviewer #1's comments:

We thank Reviewer # 1 for his thoughtful comments and suggestions that have helped to improve this manuscript. Our responses to comments (in bold style) and the corresponding changes to the manuscript are detailed below.

The revised manuscript by Peng et al. is much approved, and I thank the authors for the efforts to address my review. I believe the revised paper is suitable for publication. Only two questions still in need of attention.

1.Table 1, lines 503-516,Could you mention that expC has better RMSE and CORR than expJ in JJJ and reasons for this?

It is interesting to note that expC has better RMSE and CORR than expJ but poor bias in JJJ. And expC has better bias and RMSE than expJ but poor CORR in PRD. Maybe small number of samples caused the uncertainties of the statics. However, the differences were very small. The analysis of both experiments were very similar.

We have added some discussions in Lines 536-539

2.Revised figure 4(c),I believe that both Figure 4 in the previous manuscript and Figure 4(e) in the revised manuscript shows PM2.5 mass difference (assimilation minus control) for expJ. However, distribution is different before and after the revise; negative increments over India and Southeast Asia are disappeared in the revised one.

I am sorry that I have changed the figure in the revised manuscript. In ACPD, Figure 4 was assimilation minus control (see ReFig. 1). In the revised manuscript, Figure 4e was increment, assimilation minus background. They are not the same.

We have added some discussions in Lines 545-551 for the negative PM2.5 mass difference (assimilation minus control) over India and Southeast

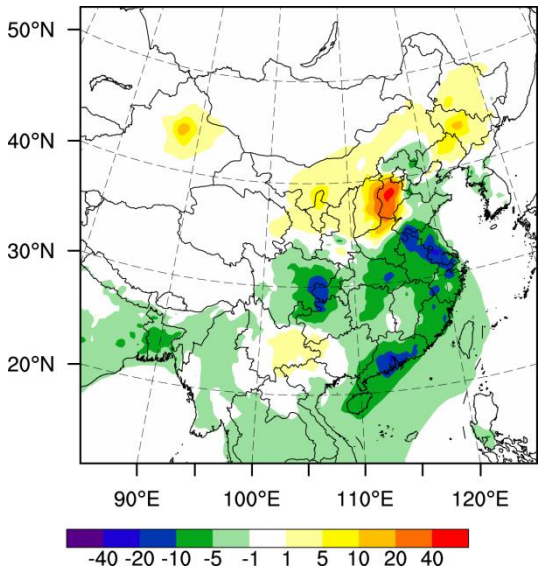

ReFig. 1(same as figure 4 in ACPD. $PM_{2.5}$ mass differences (assimilation minus control, μg m^{-3}) at the lowest model level averaged over all hours from 6 to 16 October 2014.

Response to Reviewer #3's comments:

We thank Reviewer # 3 for their thoughtful comments and suggestions that have helped to improve this manuscript. Our responses to comments (in bold style) and the corresponding changes to the manuscript are detailed below.

The authors present the results of a forecasting system that assimilates both initial hourly aerosol concentration and emission fluxes in order to improve the forecasting of particulate matter concentrations over China. To evaluate the performance of this system the forecasted concentrations are contrasted on one hand with independent observations not assimilated by the system and on the other hand against a control run without any assimilation and a forecast experiment only assimilating initial conditions but no emissions. The forecast is conduct for all China but a more in depth analysis is conducted in three regions experiencing stronger pollution levels. These three regions are the Beijing-Tianjin-Hebei region, the Yangtze River delta and the Pearl River Delta. The authors present results illustrating that the forecast assimilating initial conditions and emissions performs much better than the control simulation. Performance analysis in the three above-mentioned regions suggests that the system achieves improvements for almost all 48-h forecast in two of them while in the third one the improvement is more limited. Similarly the performance of the joint assimilation compared to the one only assimilating initial conditions shows improvement in two of the regions.

The results presented in the manuscript are interesting, however the authors conduct only a shallow analysis of the results and do not discuss how some of the assumptions made in the system affect the result. Although I recommend this paper for publication I would suggest the authors extend the discussion of the results addressing some of the topics highlighted below. When presenting a new inversion system, in addition of presenting the main results (if it works or not), the limitations of the system and their impact should also be presented.

General comments

The authors assume prior emissions constant in time but it is well known that emissions are not constant throughout the day. Why were emissions considered constant throughout the day and also throughout the week? How much of the improvement in performance of the system comes from this assumption? How much better does the control perform when variable emissions within the day are allowed? Furthermore, the implications of not perturbing emissions of elemental carbon and organic carbon should be included in the manuscript. How does this affect the forecast? How realistic is the result provided by the system with this constrain?

It is true that emissions are not constant throughout the day. As also found in earlier modeling studies, the temporal allocation of emissions plays essential roles for chemical forecasts (de Meij et al., 2006; Wang et al, 2009). However, it still lacks resolution of temporal allocations at shorter but critical (e.g.,day-of-week, diurnal) scales. In order to keep objective for the prior anthropogenic emissions, no time variation was added in this work. However, vertical allocations of anthropogenic emissions are considered. The power generator emissions were interpolated for the lowest eight vertical levels (Woo et al., 2003; de meij et al., 2006; Wang et al., 2010). Other anthropogenic emissions were assigned totally to the 1^{st} level.

The constant anthropogenic emissions will worsen the chemical forecasts of the control run. Wang et al. (2010) pointed that surface NO_2 and SO_2 concentrations are reduced by respectively 3-7 and 6-12 ppbv over major cities and industrial areas when the emissions are allocated temporally and spatially. And surface O_3 concentrations are higher by 4-8 ppbv at night and 2-4 ppbv in daytime over broad areas of northern, eastern and central China. For the joint DA system itself, it cannot benefit from the constant prior anthropogenic emissions. But the normalized RMSE in Figure 10g decreased due to the poor forecasts of control run. The control run will perform better when variable emissions within the day are allowed, especially during the night. As a result, the relative reduction in RMSE could not be so large during the night.

The above discussions are added in Lines 761-770.

For the assimilation of $\mathbf{BC_1}$, $\mathbf{BC_2}$, $\mathbf{OC_1}$ and $\mathbf{OC_2}$, the difference between expC and expJ can be seen as the perturbing emissions of $\mathbf{E}_{\mathrm{EC}}$ and $\mathbf{E}_{\mathrm{ORG}}$ since $\mathbf{E}_{\mathrm{EC}}$ and $\mathbf{E}_{\mathrm{ORG}}$ of the anthropogenic emissions were not assimilated in expJ. ReFig. 1 and ReFig. 2 show mass differences (assimilation minus control, $\mu g\ m^{-3}$) at the lowest model level averaged over all hours from 6 to 16 October 2014 in expJ and expE respectively for $\mathbf{BC_1}$, $\mathbf{BC_2}$, $\mathbf{OC_1}$ and $\mathbf{OC_2}$. Though we cannot conclude which one is closer to the truth due to the lack of observations, $\mathbf{OC_1}$ and $\mathbf{OC_2}$ are changed contributed to the $PM_{2.5}$ assimilation in both experiments, which suggests that the influence of not perturbing $\mathbf{E}_{\mathrm{EC}}$ and $\mathbf{E}_{\mathrm{ORG}}$ could be negligible. The reason that the differences of $\mathbf{BC_1}$ and $\mathbf{BC_2}$ are close to zero is that the magnitude of $\mathbf{BC_1}$ and $\mathbf{BC_2}$ are too small.

The above discussions are added in Lines 775-781

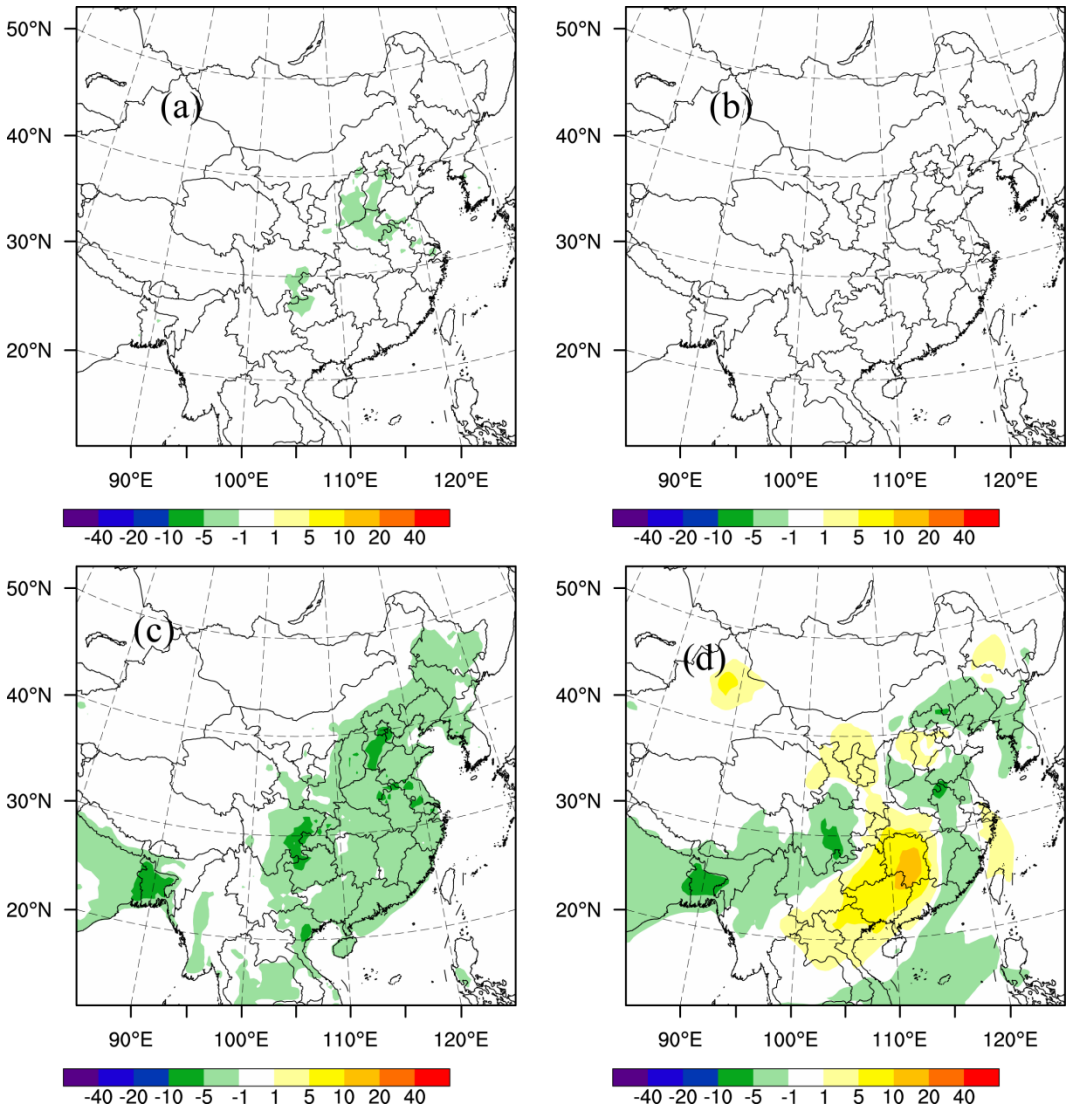

ReFig. 1. (a) $\mathbf{BC_1}$; (b) $\mathbf{BC_2}$; (c) $\mathbf{OC_1}$ and (d) $\mathbf{OC_2}$ mass differences (assimilation minus control, μg m^{-3}) at the lowest model level averaged over all hours from 6 to 16 October 2014 in expJ.

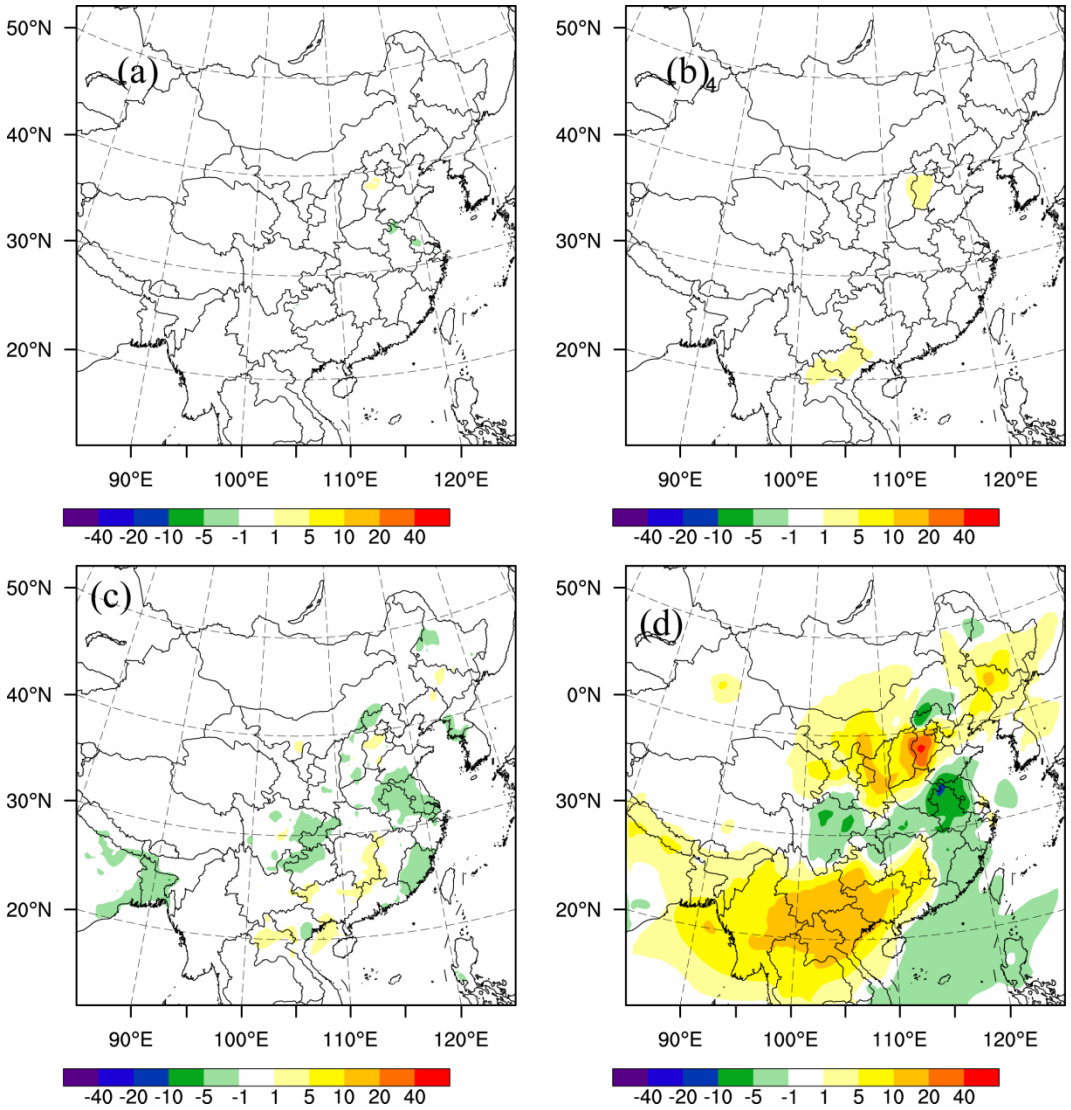

ReFig. 2. (a) $\mathbf{BC_1}$; (b) $\mathbf{BC_2}$; (c) $\mathbf{OC_1}$ and (d) $\mathbf{OC_2}$(a) $\mathbf{BC_1}$; (b) $\mathbf{BC_2}$; (c) $\mathbf{OC_1}$ and (d) $\mathbf{OC_2}$ mass differences (assimilation minus control, μg m^{-3}) at the lowest model level averaged over all hours from 6 to 16 October 2014 in expE.

The authors examine first the performance of the system by comparing the analysis of both assimilation experiments (expC and expJ) to the observations and then the forecast. It is interesting to note that when the analysis of both experiments are examined a better performance is obtained in PRD and JJJ when only initial conditions (IC) are assimilated (i.e. expC). However, when comparing the forecasts between both experiments, expJ performs better than the forecast of expC. What are the implications of this result? Furthermore, the authors provide a too simplistic analysis of the performance of the forecast in the

three regions. Yes it is true that expJ improves with respect to the control and expC in YRD and PRD, but this is mostly for daytime, during night-time the improvement is very similar in three regions. In YRD, the performance is actually deteriorated during nighttime and in JJJ there is either deterioration or no improvement after 24 hr forecast for both assimilation experiments. Although the authors suggest that this is mainly to a good performance of the model during nighttime, this is not enough I believe. Why is the performance of the control run better during night? Why does the assimilation have so little impact during night? Why should the model have better performance for nocturnal conditions? Was it tuned under such conditions? Do the a priori emissions provided, the ones considered constant, correspond to night emissions? I would suggest the authors spend a bit more trying to address this issue as they have done so far.

From Table 1, the biases were -10.3, -1.6 and 4.7μg $m^{-3}$for JJJ, YRD and PRD, respectively, and RMSEs were 66.9, 15.3, 16.1μg m^{-3} respectively in expJ. The biases were -12.2, -2.4 and -2.3μg $m^{-3}$for JJJ, YRD and PRD, respectively, and RMSEs were 64, 17.3, 15.6μg m^{-3} respectively, in expC. Thus, expC has better RMSE and CORR than expJ but poor bias in JJJ. And expC has better bias and RMSE than expJ but poor CORR in PRD. Maybe small number of samples caused the uncertainties of the statics. However, the differences were very small. The analysis of both experiments were very similar.

. When comparing the forecasts between both experiments, expJ performed much better than the forecast of expC. This could be attributed much to the emissions since the ICs of both forecasts were very similar. In the forecast experiment of expC, the emissions were the default monthly anthropogenic emissions. While in the forecast experiment of expJ, the assimilated emissions were different much from the default monthly anthropogenic emissions (see Figure 5 and 6). Also, there was diurnal variation.

The above discussions are added in Lines 536-539 and Lines 721-726

The improvements were comparatively small in PRD in the daytime. And the performance was actually deteriorated in YRD during the same time. One of the possible reasons was that chemical model performed sufficiently well during daytime when the boundary layer was unstable and therefore the further improvement was more difficult. And there were always large errors during the night when the boundary layer was stable, so that large improvements could be obtained. The other possible reason can be attributed to the a priori constant emissions. The differences between the optimized $PM_{2.5}$ emissions and the prior emissions were comparatively small during the day, but the optimized $PM_{2.5}$ emissions were much smaller than the a prior emissions during the night. So that the control run could performed worse during the night and it could performed well during the day. Given the a priori variable emissions provided, the control run will perform better during the night.

We have added the above discussions in Lines 680-690

If the difference between the control run and expC can be seen as the contribution of assimilating concentrations, can the difference between expC and expJ as the impact of assimilating emissions? If so, is it really worth if to assimilate both? Why wasn't there and expE conducted where only emissions were assimilated? Figure 8 suggests that in most of the days in the three cities, the fact of assimilating only IC has little impact on the forecast. Figure 9 also illustrates that most of the improvement comes when emissions are assimilated. What if only emissions were to be assimilated, could that be enough? I suggest the authors include a discussion section where this is addressed.

The difference between the control run and expC can be seen as the contribution of assimilating concentrations, and the difference between expC and expJ can be seen as the impact of assimilating emissions. Though the fact of assimilating only IC has little impact on the forecast in most of the days in the three cities (See Figure 9) and most of the improvement comes when emissions are assimilated (See Figure 10), it was still worth to simultaneously assimilate the chemical ICs and emission. We have performed the expE for 7 days where only emissions were assimilated during our

limited time. In order to remove the influence of the cumulative errors resulting from the initialization and spin-up experiment, the chemical ICs were first assimilated from 2000 UTC to 2300 UTC 4 October 2014. The first 50 ensemble chemical fields were drawn from the WRF-Chem ensemble forecasts valid at 2000 UTC 4 October 2014. Then expE were performed from 0000 UTC 5 October 2014 to 0000 UTC 12 October 2014.

In expE, the chemical concentrations can be updated by the WRF-Chem model simulations with the assimilated emissions as the initial field in each DA cycle (see ReFig. 3). That means that the 50-member ensemble forecasts were performed twice and it was time consuming.

On the other hand, it seemed that better concentration analysis could be obtained in expJ due to the simultaneous assimilation of ICs and emissions. Both the background $PM_{2.5}$ and the analysis $PM_{2.5}$ in the assimilation experiments were comparatively near to the observations (see ReFig. 4) in expJ. However, both the background and the analysis $PM_{2.5}$ deviated markedly from the observations (see ReFig. 5) in expE. Especially in Beijing, the performance is deteriorated for $PM_{2.5}$ observations above 200 μg m^{-3} when an intense pollution events occurred. This will lead to larger uncertainties for the emission inversion. Also the improvement of $PM_{2.5}$ forecasts will be limited due to the comparatively poor chemical ICs.

We added a **discussion in Lines 781-792**

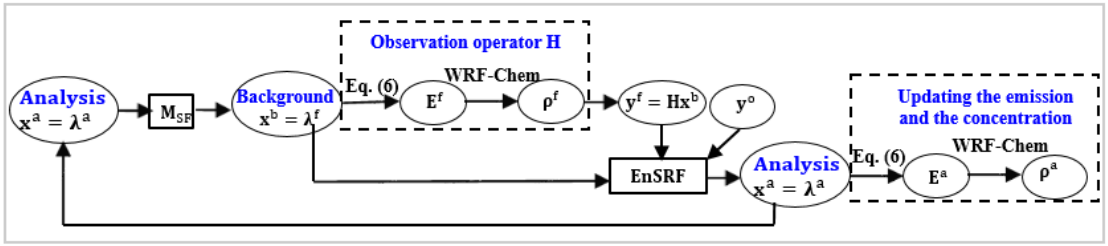

ReFig. 3 Flow chart of the DA system of expE

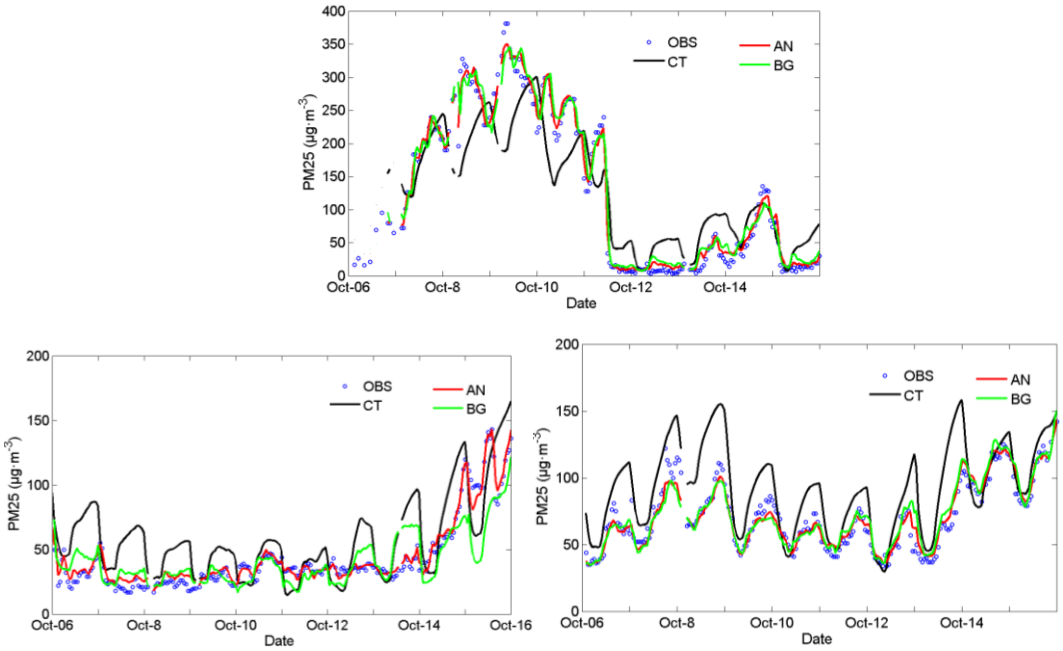

ReFig. 4. Time series of the hourly $PM_{2.5}$ obtained from observations (circle), control run (black line), analysis (red line), and background (green line) in three megacities: (a) Beijing; (b) Shanghai; and (c) Guangzhou in expJ.

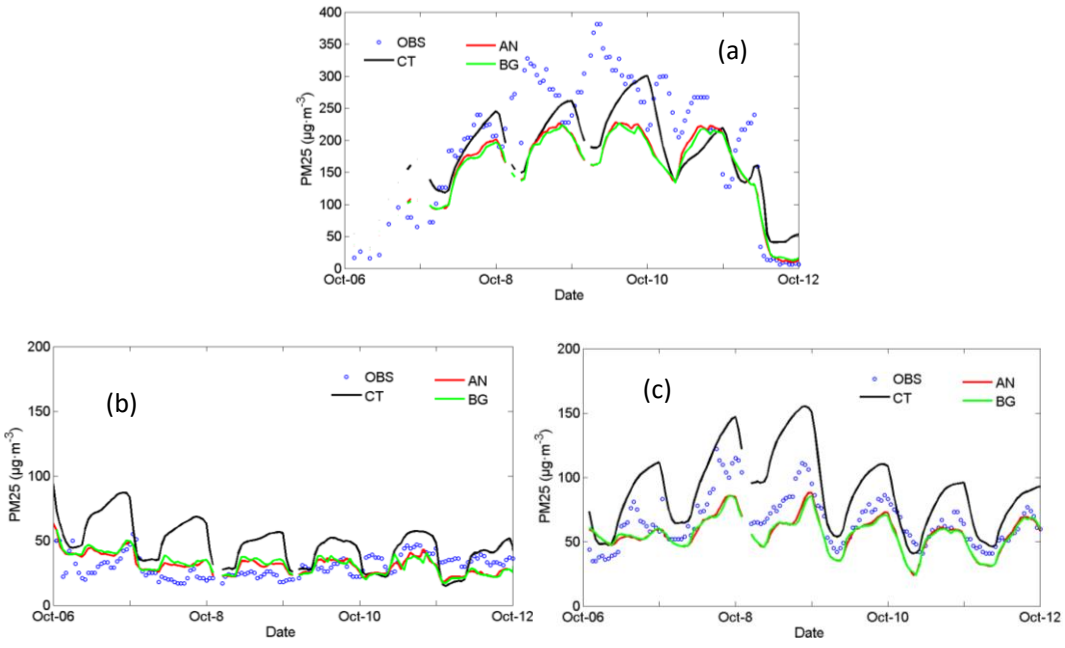

ReFig. 5. Time series of the hourly $PM_{2.5}$ obtained from observations (circle), control run (black line), analysis (red line), and background (green line) in three megacities: (a) Beijing; (b) Shanghai; and (c) Guangzhou in expE.

The assimilations system needs further description. The authors describe how the observation error covariance matrix (R) is defined but do not do the

same for the background error covariance matrix (Pb). How is Pb defined? The authors should explain this in the manuscript. Furthermore, observations from 77 stations were assimilated and observations from another set of 77 stations were used for verification purposes. However, in the three regions of interest in the manuscript; namely JJJ, YRD, and PRD, it is not clear how many stations were assimilated and how many were used in the verification. This number is provided in the caption of Figure 1 but should also be included in the text. Please also clarify if all these verification stations are used to compute the statistics presented in Figure 9.

$\mathbf{P}^b$ is defined in Line 241.

We have added the numbers of the stations used for assimilation and those for verification in the three regions in lines 489-492.

All these verification stations are used to compute the statistics presented in Figure 10 and we have clarified.

Specific comments

1 Lines 30-31: Acronyms should be defined.

We have defined the acronyms in Lines 22-27

2 Lines 79-81: Structure of the paper described is not consistent with actual structure of the paper. There are 6 sections in the manuscript and only 5 according to text in last sentence of section 1.

Thanks for pointing out this mistake and we have revised in Lines 78-81.

3 Line 131: Sub index i should be defined. It is clear from the text what it stands for but should be introduced anyway.

We have defined it in Lines 131-134.

4 Line 132: Why is it t-2 for the emissions and t-1 for the concentrations (line 131)? Is it a mistake and it should be t-1 for both? If not, please explain.

Thanks for pointing out this error. I have corrected it in Line 133.

5 Please explain which criteria was applied to define the limits (0.1 and 1.25) to the spread of (Ki,t)inf. How were they defined?

In Peng et al. (2015), several sensitive experiments were performed to investigate β (10, 50, 60, 70, 75, 80, 100). The ensemble spread of $\lambda_{i,t}^{a}$ ranged from 0.05 to 1.25 for β =60, 70, 75, 80. And the CO_2 DA system worked comparatively well for β =60, 70, 75, 80. For β = 10, 50, the impact of assimilation was small due to the small ensemble spread; For β = 100 the assimilated CO_2 fluxes deviated markedly from the "true" CO_2 fluxes due to too large ensemble spread. Therefore, in this work, $\beta = 1.5$ was chosen to make ensure the ensemble spread of $(\boldsymbol{\kappa}_{i,t})_{\inf}$ ranged from 0.1 to 1.25 in this study.

We have added some explanations in Lines 148-152.

6 Line 150: Why are the negative values set to 0.001 and not simply 0? Please explain.

We have no special reasons to set the negative values as 0.001. It is also fine to set them as 0. We have added this in Lines 157-158.

7 Line 322: Remove "which is a limitation of this manuscript". It is already stated in lines 300 and 301.

We have removed this sentence.

8 Lines 352-356: Explain the criteria used to select the stations that would be used for verification and those used in the assimilation? How many of each are in the different regions. The total number of stations in each region is provided but it is not said how many of them are for validation or verification purposes.

There are altogether 906 national control measurement sites over China. The reason we did not use all the measurements is that we also have done a sensitive experiment by using $PM_{2.5}$ measurements at the five U.S. Embassies stations and

$PM_{2.5}$ measurements at 34 monitoring sites in Beijing from the national Environmental Monitoring Center except sensitive experiments by only using $PM_{2.5}$ measurements at the five U.S Embassies stations. The DA system could ingest the observations effectively by only using $PM_{2.5}$ measurements at the five U.S Embassies stations. We thought we might gain even better assimilation results in Beijing-Tianjin-Hebei region for more assimilation measurements. However, it is unexpected that the impact of the ensemble assimilation on ICs and emissions were almost negligible and no improvements were gained for $PM_{2.5}$ forecast. So far we did not know the exact reason. But, the 34 sites in Beijing are fall into 8 model grids (Chen et al., 2016). So many observations are fall into one model grids. However, Chemicals are influenced greatly by the local emissions. Observations are not in good agreement with each other though they are fall into the same model grid. Therefore, the observation error covariance matrix **R** may include much noise. And the ensemble data assimilation system at this stage could dot absorb useful observation information effectively. However, further investigations are needed to resolve the question. In this work, only a few measurements were assimilated for simplicity since the DA system performed well by only using $PM_{2.5}$ measurements at the five U.S Embassies stations.

The $PM_{2.5}$ observation sites spanned most of central and eastern China but were primarily located in urban and suburban areas. So it always happened that there are more than one observation sites in certain city. We randomly selected one observation site in a city for assimilation experiment and one for verification purposes since we did not know the exact station type. Altogether 77 stations were selected for the $PM_{2.5}$ assimilation experiment and another 77 stations were selected for verification. Among them, 12 stations were selected for assimilation and 12 stations were selected for verification in the Beijing-Tianjin-Hebei (JJJ), 24 stations were selected for assimilation and 24 stations were selected for verification in the Yangtze River delta (YRD), and 9 stations were selected for assimilation and 9 stations were selected for verification in the Pearl River delta (PRD).

We have added some explanations in Lines 361-370, and in lines 489-492.

9 Line 371: Why are hourly concentrations above 800 μg m-3 considered unrealistic? Hasn't had China intense pollution events where this limit was exceeded in terms of hourly concentration? In any case, this should be argued much better if observations are removed. Also, why are observations where the departure of the ensemble mean of the first guess exceeds 100 μg m-3 removed?

In Schwartz et al. (2012), $PM_{2.5}$ values > 200 μg m^{-3} were deemed unrealistic and were not assimilated. And observations leading to innovations exceeding 100 μg m^{-3} were also omitted. Considering that China has had intense pollution events, $PM_{2.5}$ values larger than 800 μg m^{-3} were discarded in this work. Also observations leading to innovations exceeding 100 μg m^{-3} were also omitted. The statics show that 8 observations were discarded because they were larger than 800 μg m^{-3} and 243 (around 1.5%) were discarded due to leading to innovations exceeding 100 μg m^{-3}.

We have added some explanations in Lines 386 and 389.

10 Line 408: What is the impact of considering that no correlations exist between emission variables. What is the impact on the assimilation and the forecast?

The emissions variables are related to each other. The correlations between the variables were reduced when perturbing the emissions without considering the correlations. Thus, the chemical forecast would deviate from the truth to some degree. Fortunately, the perturbed emissions were only used in the initialization and spin-up experiment and expC. Therefore, there were no impact on expJ and the control run except for expC.

We have added some explanations in Lines 770-775.

11 Lines 460-461: What is it, are the emissions perturbed or not in expC? According to this line not, but according to the statement in lines 450-452, the emissions are perturbed by adding random noise.

The emissions were perturbed by adding random noise in expC.

They were the prescribed emissions E_t^p themselves in the control experiment. So they were not perturbed. Lines 460-461 described the emissions in control experiment and they were right.

12 Lines 566-570: Where are the numbers in this paragraph coming from? Please explain and present them.

Figure 6 shows time series of emission scaling factors extracted from the ensemble mean of the analyzed λ_{NO}^a, λ_{SO2}^a and λ_{NH3}^a.

13 Line 609: Replace "analysing" with "analysis".

We have replaced "analysing" with "analysis" in Line 632.

14 Line 649: What exactly is "dramatic"? How large is that? Please replace.

We replaced "dramatic" with "very large" in Line 672.

15 Lines 1097-1101: Authors should specify if the analysis presented in the figures include all verification stations in each region or only some of them. In addition, authors should also clarify to which dates the analysis presented in the figures corresponds.

All these verification stations presented in figure 1 in each region are used to calculate the statistics from 6 to 16 October. And we have clarified in Figure 10.

Improving $PM_{2.5}$ forecast over China by the joint adjustment of initial conditions and source emissions with an ensemble Kalman filter

Zhen Peng[1,2], Zhiquan Liu[2], Dan Chen[2], Junmei Ban[2]

1 School of Atmospheric Sciences, Nanjing University, Nanjing, China

2 National Center for Atmospheric Research, Boulder, Colorado, USA

Abstract. In an attempt to improve the forecasting of atmospheric aerosols, the ensemble square root filter algorithm was extended to simultaneously optimize the chemical initial conditions and emission input. The forecast model, which was expanded by combining the Weather Research and Forecasting with Chemistry (WRF-Chem) model and a forecast model of emission scaling factors, generated both chemical concentration fields and emission scaling factors. The forecast model of emission scaling factors was developed by using the ensemble concentration ratios of the WRF-Chem forecast chemical concentrations and also the time smoothing operator. Hourly surface fine particulate matter ($PM_{2.5}$) observations were assimilated in this system over China from 5 to 16 October 2014. A series of 48-h forecasts were then carried out with the optimized initial conditions and emissions on each day at 0000 UTC and a control experiment was performed without data assimilation. Besides, we also performed an experiment of pure assimilation chemical ICs and the corresponding 48-h forecasts experiment for comparison. The results showed that the forecasts with the optimized initial conditions and emissions typically outperformed those from the control experiment. In the Yangtze River delta (YRD) and the Pearl River delta (PRD) regions, large reduction of the Root Mean Square Errors (RMSEs) was obtained for almost the entire 48-h forecast range attributed to assimilation.

Especially, the relative reduction in RMSE due to assimilation was about 37.5% at nighttime when WRF-Chem performed comparatively worse. In the Beijing–Tianjin–Hebei (JJJ) region, relatively smaller improvements were achieved in the first 24-h forecast. Comparing to the forecasts with only the optimized ICs, the forecasts with the joint adjustment were always much better for almost all the forecasts in the PRD and YRD, although they were very similar in the JJJ region.

1. Introduction

Aerosol prediction by regional air quality model in heavy polluted regions is challenging due to many factors. In addition to the deficiency of chemistries, the uncertainties of primary and precursor emissions and the initial conditions (ICs) also limit the forecast accuracy. Data assimilation (DA), which is used to improve the ICs of aerosols and to optimize data on aerosol emissions, has been shown to be one of the most effective ways to improve the forecasting of aerosol pollution.

From the perspective of reducing the uncertainties in the ICs for aerosols, recent efforts have focused on assimilating aerosol observations using optimal interpolation (Collins et al., 2001; Yu et al., 2003; Adhikary et al., 2008; Tombette et al., 2009; Lee et al., 2013) or variational (Kahnert, 2008; Zhang et al., 2008; Benedetti et al., 2009; Pagowski et al., 2010; Liu et al., 2011; Schwartz et al., 2012; Li et al., 2013; Jiang et al., 2013; Saide et al., 2013) DA algorithms. Ensemble-based DA algorithms, such as the ensemble Kalman filter (EnKF) (Sekiyama et al., 2010; Schutgens et al., 2010a, 2010b; Pagowski and Grell, 2012; Dai et al., 2014; Rubin et al., 2016; Ying, X.M., et al., 2016; Yumimoto et al., 2016) and the hybrid variational-ensemble DA approach (Schwartz et al., 2014) have also been applied to aerosol predictions. All these studies have shown that DA is one of the most effective ways of improving aerosol forecasting through assimilating aerosol observations from multiple sources (e.g. ground-based observations and satellite measurements) to update the chemical ICs.

Numerous studies have used DA approaches to estimate or improve source

emissions. The EnKF is one of the most popular DA algorithms used to improve estimates of aerosols and gas-phase emissions, such as NO_x, volatile organic compounds, and SO_2 (van Loon et al., 2000; Heemink and Segers, 2002; Zhang et al., 2005; Barbu et al., 2009; Sekiyama et al., 2010; Huneeus et al., 2012; Schutgens et al., 2012; Huneeus et al., 2012, 2013; Miyazaki et al., 2014). Variational DA algorithms have also been applied to constrain emissions of air pollution, such as black carbon, organic carbon, dust, NH_3, SO_x and NO_x (Hakami et al., 2005; Elbern et al., 2007; Henze et al., 2007, 2009; Yumimoto et al., 2007, 2008; Dubovik et al., 2008; Wang et al., 2012; Guerrette and Henze, 2015). These studies have indicated that DA can efficiently reduce the uncertainty in the emission inventories and lead to improvements in the forecasting of air quality (Mijling and van der A, 2012).

The optimization of chemical ICs and pollution emissions can improve aerosol forecasts and therefore further improvements are likely to be achieved by simultaneously optimizing the chemical ICs and emissions. Tang et al. (2011) reported that the simultaneous adjustment of the ICs of O_3, NO_x and volatile organic compounds and the emissions of NO_x and volatile organic compounds produced overall better performance in both the 1-h and 24-h ozone forecasts than the adjustment of pure ICs or emissions. Miyazaki et al. (2012) reported that the simultaneous adjustment of emissions and concentrations is a powerful approach to correcting the tropospheric ozone budget and profile analyses.

We developed a system to adjust the chemical ICs and source emissions jointly within an EnKF system coupled to the Weather Research and Forecasting with Chemistry (WRF-Chem) model (Grell et al., 2005). We then applied this system to assimilate hourly surface $PM_{2.5}$ measurements over China in early October 2014.

The remainder of the paper is organized as follows. Section 2 describes this DA system in detail and Section 3 describes the $PM_{2.5}$ observations. Then the experimental designs are introduced in Section 4. Finally, the surface $PM_{2.5}$ observations assimilation results are presented in section 5 before concluding in section 6.

2. Methodology

2.1 Forecast model

For a chemical model like WRF-Chem, the emissions are the model forcing (or boundary condition), rather than model states. Therefore, a forecasting model, **M**, was developed to forecast the emission scaling factors (representing emissions) as well as the aerosol concentrations. This model combines the WRF-Chem model and the forecast model of emission scaling factors.

2.1.1 WRF-Chem model

Version 3.6.1 of the WRF-Chem model (Grell et al., 2005) was used to forecast the aerosol and chemical species. WRF-Chem is an online model with the fully coupled chemical and meteorological components.

Most of the WRF-Chem settings were the same as those reported in Liu et al. (2011): the Goddard Chemistry Aerosol Radiation and Transport (GOCART) aerosol scheme coupled with the Regional Atmospheric Chemistry Mechanism for gaseous chemical mechanisms; the WRF single-moment five-class microphysics scheme; the Rapid Radiative Transfer Model longwave and Goddard shortwave radiation schemes; the Yonsei University (YSU) boundary layer scheme; the Noah land surface model; and the Grell-3D cumulus parameterization. For the GOCART aerosol scheme, the aerosol species include 14 defined aerosol species and a 15^{th} variable representing unspectiated aerosol contributions (P_{25}). The 14 defined aerosol species are sulfate, hydrophobic and hydrophilic organic carbon (OC_1 and OC_2, respectively), hydrophobic and hydrophilic black carbon (BC_1 and BC_2, respectively), dust in five particle size bins (effective radii of 0.5, 1.4, 2.4, 4.5 and 8.0 μm; referred to as D_1, D_2, D_3, D_4 and D_5, respectively) and sea salt in four particle size bins (effective radii of 0.3, 1.0, 3.25 and 7.5 μm for dry air; referred to as S_1, S_2, S_3 and S_4, respectively).

Figure 1 illustrates the model computational domain. It has 120*120 horizontal grid scales at a 40.5 km spacing by the lambert conform map projection centered at (35°N, 105°E). There are 57 vertical levels with the model top at 10 hPa, about 12

layers within the planetary boundary layer (among them the lowest 8 layers were under 500 m), and the first layer centered at ~12 m.

With respect to the emissions, the hourly prior anthropogenic emissions were based on the monthly regional emission inventory in Asia (Zhang et al., 2009) for the year 2006 interpolated to the model grid. The power generator emissions were interpolated for the lowest eight vertical levels (Woo et al., 2003; de meij et al., 2006; Wang et al., 2010). Other anthropogenic emissions were assigned totally to the 1st level. Emissions are very small above 500 m for all pollutants. In order to keep objective for the prior anthropogenic emissions, no time variation was added. Thus, the hourly prior anthropogenic emissions were constant. The biogenic (Guenther et al., 1995), dust (Ginoux et al., 2001), dimethylsulfide and sea salt emissions (Chin et al., 2000, 2002) were calculated online.

2.1.2 Forecast model of scaling factors

As no suitable dynamic model was available to forecast the emission scaling factors, a persistence forecasting operator served as the forecast model for the scaling factors, similar to the method used by Peng et al. (2015) for CO_2 emission inversion. Figure 2a shows the flowchart for the persistence forecasting operator $\mathbf{M}_{\mathrm{SF}}$.

If the ensemble members of the updated chemical fields $\mathbf{C}^{\mathrm{a}}_{i,t-1}$ (the subscript i refers to the ith ensemble member, the superscript a refers to the analysis, and t refers to the time) and the forecast emissions $\mathbf{E}^{\mathrm{f}}_{i,t-1}$ (the superscript f refers to the forecast) in the previous assimilation cycle are known, then the chemical fields $\mathbf{C}^{\mathrm{f}}_{i,t}$ at time t can be generated via WRF-Chem (Figure 2b). In the actual process, $\mathbf{C}^{\mathrm{f}}_{i,t}$ were available in the previous assimilation cycle, so we did not need to perform the ensemble forecasts again. A dotted box was used in Figure 2a to indicate that the ensemble forecasts were not performed in real process. The ensemble concentration ratios $\boldsymbol{\kappa}_{i,t}, (i = 1, \dots, N)$ are then calculated using

$$\boldsymbol{\kappa}_{i,t} = \frac{\mathbf{C}^{\mathrm{f}}_{i,t}}{\overline{\mathbf{C}^{\mathrm{f}}_{t}}}, (i = 1, \dots, N), (1)$$

where $\overline{\mathbf{C}^{\mathrm{f}}_{t}} = \frac{1}{N}\sum_{i=1}^{N} \mathbf{C}^{\mathrm{f}}_{i,t}$ is the ensemble mean of the forecast. The ensemble mean of

$\boldsymbol{\kappa}_{i,t}$ is,

$$\overline{\boldsymbol{\kappa}_t} = \frac{1}{N}\sum_{i=1}^{N} \boldsymbol{\kappa}_{i,t} = \frac{1}{N}\sum_{i=1}^{N} \mathbf{C}_{i,t}^{\mathrm{f}} / \overline{\mathbf{C}_t^{\mathrm{f}}} = 1, \quad (2)$$

so $\boldsymbol{\kappa}_{i,t}$ are numbers distributed around 1 and with ensemble mean values of 1.

The ensemble spreads of $\boldsymbol{\kappa}_{i,t}, (i = 1, \dots, N)$ may be small and therefore covariance inflation is used to maintain them at a certain level:

$$(\boldsymbol{\kappa}_{i,t})_{\mathrm{inf}} = \beta\left(\boldsymbol{\kappa}_{i,t} - \overline{\boldsymbol{\kappa}_t}\right) + \overline{\boldsymbol{\kappa}_t}, (i = 1, \dots, N), \quad (3)$$

In Peng et al. (2015), the CO_2 DA system worked comparatively well when the ensemble spread of $\lambda_{i,t}^{a}$ ranged from 0.05 to 1.25 for β =60, 70, 75, 80. The assimilated CO2 fluxes deviated markedly from the "true" CO2 fluxes when the ensemble spread of $\lambda_{i,t}^{a}$ were too small for β =10, 50 or when the ensemble spread of $\lambda_{i,t}^{a}$ were too large for β =100. Therefore, in this work, $\beta = 1.5$ was chosen to make ensure the ensemble spread of $(\boldsymbol{\kappa}_{i,t})_{\mathrm{inf}}$ ranged from 0.1 to 1.25. Same as $\boldsymbol{\kappa}_{i,t}$, the ensemble mean values of $(\boldsymbol{\kappa}_{i,t})_{\mathrm{inf}}$ are 1. It is noted that perhaps there are very few negative values for $(\boldsymbol{\kappa}_{i,t})_{\mathrm{inf}}$ after inflation. A quality control procedure is performed for $(\boldsymbol{\kappa}_{i,t})_{\mathrm{inf}}$ before further appliance. All these negative data were set as 0.001 in this work. There was no special reason to set them as 0.001. It is also fine to set them as 0. Then $(\boldsymbol{\kappa}_{i,t})_{\mathrm{inf}}$ were re-centered to ensure the ensemble mean values of $(\boldsymbol{\kappa}_{i,t})_{\mathrm{inf}}$ were all 1.

As the concentrations were closely related to the emissions both locally and in the upwind regions and there is no suitable dynamic model available to forecast the emission scaling factors, the inflated concentration ratios $(\boldsymbol{\kappa}_{i,t})_{\mathrm{inf}}$ serve as the prior emission scaling factors $\boldsymbol{\lambda}_{i,t}^{\mathrm{p}}$:

$$\boldsymbol{\lambda}_{i,t}^{\mathrm{p}} = (\boldsymbol{\kappa}_{i,t})_{\mathrm{inf}}, (i = 1, \dots, N), \quad (4)$$

The above equation is not supported according to the mass conservation equation but just for the purpose to generate the ensemble emissions. Same as $(\boldsymbol{\kappa}_{i,t})_{\mathrm{inf}}$, $\boldsymbol{\lambda}_{i,t}^{\mathrm{p}}$ are numbers distributed around 1. From the perspective of generating the ensemble emissions, they can play the same role

as other data, such as the random numbers created by using the standard normal distribution function. However, there are correlations among the grid-points of $(\boldsymbol{\kappa}_{i,t})_{\text{inf}}$ because $(\boldsymbol{\kappa}_{i,t})_{\text{inf}}$ are calculated through a short-term forecast of WRF-Chem. Thus, $\boldsymbol{\lambda}_{i,t}^{\text{p}}$ have the same correlations as $(\boldsymbol{\kappa}_{i,t})_{\text{inf}}$. While, the random numbers are totally different. There are no correlations unless they are generated under certain correlations.

To incorporate the useful information from the previous times, the previous DA cycles' analysis scaling factors, $\boldsymbol{\lambda}_{i,t-M+1}^{\text{a}}$, ⋯, $\boldsymbol{\lambda}_{i,t-2}^{\text{a}}$, $\boldsymbol{\lambda}_{i,t-1}^{\text{a}}$ and the prior scaling factor $\boldsymbol{\lambda}_{i,t}^{\text{p}}$ were used to estimate $\boldsymbol{\lambda}_{i,t}^{\text{f}}$ by the time smooth operator; namely,

$$\boldsymbol{\lambda}_{i,t}^{\text{f}} = \frac{1}{M}\left(\sum_{j=t-M+1}^{t-1}\boldsymbol{\lambda}_{i,j}^{\text{a}} + \boldsymbol{\lambda}_{i,t}^{\text{p}}\right), (\, i = 1, \dots, N, j = t-M+1, \dots, t-1), \quad (5)$$

Here, M is the time window of the smooth operator. In this study, a value of $M = 4$ (hours) was chosen. According to the smooth operator, the ensemble mean values of $\boldsymbol{\lambda}_{i,t}^{\text{f}}$ depend on the ensemble mean of $\boldsymbol{\lambda}_{i,t-M+1}^{\text{a}}$, ⋯, $\boldsymbol{\lambda}_{i,t-2}^{\text{a}}$, $\boldsymbol{\lambda}_{i,t-1}^{\text{a}}$, $\boldsymbol{\lambda}_{i,t}^{\text{p}}$, where the ensemble means of $\boldsymbol{\lambda}_{i,t}^{\text{p}}$ are all 1. After multiple iterations, the smooth operator can give comparatively good estimation for $\boldsymbol{\lambda}_{i,t}^{\text{f}}$ since anthropogenic emissions are stable at a certain time scale (Mijling et al., 2012). It is a compromise between prescribed prior emissions and letting the system propagate all observation information from one step to the next without any guidance (Peters et al., 2007), for the case $M = 4$.

The ensemble members of the emissions were calculated according to

$$\mathbf{E}_{i,t} = \boldsymbol{\lambda}_{i,t}\mathbf{E}_{t}^{\text{p}}, (i = 1, \dots, N), \quad (6)$$

where $\mathbf{E}_{i,t}$ is the ith ensemble member of the emissions for each grid at time t, $\boldsymbol{\lambda}_{i,t}$ represents the scaling factors and $\mathbf{E}_{t}^{\text{p}}$ is the prescribed emission, which can be obtained from the emission inventories. It is noted that the correlations among the grid-points of the prior emissions depend on $\boldsymbol{\lambda}_{i,t}^{\text{p}}$. These correlations may deviate far from the truth but we have no other suitable substitute. However, the correlations among the grid-points of the forecast emissions should be more or less close to the truth due to the appliance of the smooth operator after multiple iterations.

It is noted although the method is very similar to that used by Peters et al. (2007) and Peng et al. (2015) for CO_2 emission inversion, it is still of novelty for applications

in aerosol anthropogenic emissions. In Peters et al. (2007), $\boldsymbol{\lambda}_{i,t}^{\mathrm{p}}$ were all 1. And only natural CO_2 emissions (i.e., biospheric and oceanic emissions) were assimilated at the ecological scale due to the 'signal-to-noise' problem. Thus, the uncertainty of anthropogenic and other CO_2 emissions were ignored. Besides, the framework is more advanced compared to our previous work. In Peng et al. (2015), in order to generate $\boldsymbol{\lambda}_{i,t}^{\mathrm{p}}$, a set of ensemble forecasts were performed from time *t* to *t*+1 to produce the CO_2 concentration fields, forced by the prescribed net CO_2 surface fluxes with the previous assimilated concentration fields as initial conditions. That means that the ensemble forecast were performed twice in that DA system and it was time consuming. However, in order to save computing time, we used the chemical fields $\mathbf{C}_{i,t}^{\mathrm{f}}$ available in the previous assimilation cycle to calculate $\boldsymbol{\lambda}_{i,t}^{\mathrm{p}}$ in this work. Thus, WRF-Chem runs to forecast only once during a DA cycle.

2.2 Ensemble square root filter

The ensemble square root filter (EnSRF) algorithm was introduced by Whitaker and Hamill (2002) and its expansion to analyzing aerosol ICs was described by Schwartz et al. (2014). The traditional EnKF with perturbed observations (Evensen 1994) introduces sampling errors by perturbing the observations. In contrast to the traditional EnKF, the EnSRF (Whitaker and Hamill, 2002) and the Ensemble Adjustment Kalman Filter (EAKF, developed by Anderson, 2001) obviate the need to perturb the observations. The local ensemble Kalman filtering (LEKF), a kind of EnSRF, was presented by Ott et al. (2002, 2004). It was computationally more efficient compared to the traditional EnKF, since it simultaneously assimilates the observations within a spatially local volume independently. The local Ensemble Transform Kalman Filter (LETKF, Hunt, 2007) integrates the advantages of the Ensemble Transform Kalman Filter (ETKF, developed by Bishop et al., 2001) and the LEKF. The computational cost of LETKF is much lower than that of the original LEKF because the former does not require an orthogonal basis. Though LETKF has

more advantages, we still chose the same EnSRF as Schwartz et al. (2014) because we did not need to extend it to analyzing aerosol ICs, very similar to Schwartz et al. (2014).

Following the notation of Ide et al. (1997), given an *m*-dimensional background model forecast vector $\mathbf{x}^{\mathrm{b}}$, a *p*-dimensional observation vector $\mathbf{y}^{\mathrm{o}}$ and an operator $\mathbf{H}$ that converts the model state to the observation states, we expressed the variables as an ensemble mean (denoted by an over-bar) and a deviation from the mean (denoted by a prime). Thus, the ensemble mean $\bar{\mathbf{x}}^{\mathrm{a}}$ of the analyzed state $\mathbf{x}^{\mathrm{a}}$ and the deviations $\mathbf{x}'^{\mathrm{a}}$ from the ensemble mean are updated separately by

$$\bar{\mathbf{x}}^{\mathrm{a}} = \bar{\mathbf{x}}^{\mathrm{b}} + \mathbf{K}(\mathbf{y}^{\mathrm{o}} - \mathbf{H}\bar{\mathbf{x}}^{\mathrm{b}}), \quad (7)$$

$$\mathbf{x}'^{\mathrm{a}} = \mathbf{x}'^{\mathrm{b}} + \widetilde{\mathbf{K}}(\mathbf{y}'^{\mathrm{o}} - \mathbf{H}\mathbf{x}'^{\mathrm{b}}), \quad (8)$$

where $\mathbf{K}$ is the traditional Kalman gain matrix and $\widetilde{\mathbf{K}}$ is the gain used to update the deviations from the ensemble mean. These are given by

$$\mathbf{K} = \mathbf{P}^{\mathrm{b}}\mathbf{H}^{\mathrm{T}}(\mathbf{H}\mathbf{P}^{\mathrm{b}}\mathbf{H}^{\mathrm{T}} + \mathbf{R})^{-1}, \quad (9)$$

$$\widetilde{\mathbf{K}} = \mathbf{P}^{\mathrm{b}}\mathbf{H}^{\mathrm{T}}\left[\left(\sqrt{\mathbf{H}\mathbf{P}^{\mathrm{b}}\mathbf{H}^{\mathrm{T}} + \mathbf{R}}\right)^{-1}\right]^{\mathrm{T}}\left(\sqrt{\mathbf{H}\mathbf{P}^{\mathrm{b}}\mathbf{H}^{\mathrm{T}} + \mathbf{R}} + \sqrt{\mathbf{R}}\right)^{-1}$$

$$= \left(\mathbf{1} + \sqrt{\mathbf{R}/(\mathbf{H}\mathbf{P}^{\mathrm{b}}\mathbf{H}^{\mathrm{T}} + \mathbf{R})}\right)^{-1}\mathbf{K}, \quad (10)$$

where $\mathbf{P}^{\mathrm{b}} = \frac{1}{N-1}\sum_{i=1}^{N}\mathbf{x}'^{\mathrm{b}}(\mathbf{x}'^{\mathrm{b}})^{T}$ is the $m * m$ -dimensional background error covariance matrix and $\mathbf{R}$ is the $p * p$-dimensional diagonal observation error covariance matrix. In real applications, $\mathbf{P}^{\mathrm{b}}\mathbf{H}^{\mathrm{T}}$and $\mathbf{H}\mathbf{P}^{\mathrm{b}}\mathbf{H}^{\mathrm{T}}$ will be approximated using the background ensemble; namely,

$$\mathbf{P}^{\mathrm{b}}\mathbf{H}^{\mathrm{T}} = \frac{1}{N-1}\sum_{i=1}^{N}\mathbf{x}'^{\mathrm{b}}(\mathbf{H}\mathbf{x}'^{\mathrm{b}})^{T} \quad (11)$$

$$\mathbf{H}\mathbf{P}^{\mathrm{b}}\mathbf{H}^{\mathrm{T}} = \frac{1}{N-1}\sum_{i=1}^{N}\mathbf{H}\mathbf{x}'^{\mathrm{b}}(\mathbf{H}\mathbf{x}'^{\mathrm{b}})^{T}. \quad (12)$$

In equations (11) and (12), N is the ensemble size.

Note that for the joint analysis of ICs and emissions, the state vector $\mathbf{x}$ is the joint vector of the mass concentration $\mathbf{C}$ and the emission scaling factor $\boldsymbol{\lambda}$, i.e. $\mathbf{x} = [\mathbf{C}, \boldsymbol{\lambda}]^{\mathrm{T}}$. In this study, the state variables of the analysis of the ICs were the 15 WRF-Chem/GOCART aerosol variables, same as that reported by Schwartz et al. (2012). The state variables of the emission scaling factors include $\boldsymbol{\lambda}_{\mathrm{PM2.5}}$, $\boldsymbol{\lambda}_{\mathrm{SO2}}$, $\boldsymbol{\lambda}_{\mathrm{NO}}$

and $\boldsymbol{\lambda}_{\mathrm{NH3}}$ and are described in section 2.3.1. After each ensemble analysis, the ensemble forecasts were performed with the corresponding models to advance $\mathbf{C}$ and $\boldsymbol{\lambda}$ to the next analysis time.

In this work, a 50-member ensemble was chosen, following Schwartz et al. (2012) and Whitaker and Hamill (2002). Covariance localization forced EnSRF analysis increments to zero 1280 km from an observation in the horizontal and one scale height to reduce spurious correlations due to sampling error for all control variables, similar to Pagowski et al., (2012) and Schwartz et al., (2012, 2014). In addition, posterior (after assimilation) multiplicative inflation following Whitaker and Hamill (2012) was applied aiming to maintain ensemble spread for only the concentration analysis. The inflation factor $\alpha = 1.2$ was chosen as Pagowski et al., (2012) and Schwartz et al., (2012, 2014). Additive or prior inflation was not employed. As for the emission scaling factor $\boldsymbol{\lambda}$, the inflation was not used at this step.

2.3 Data assimilation system

2.3.1 State variables

As stated in section. 2.2, the state variables of the analysis of the ICs were the 15 WRF-Chem/GOCART aerosol variables. The $PM_{2.5}$ observation operator was the same as that described by Schwartz et al. (2012) and expressed as

$$\mathbf{y}^{\mathrm{f}} = \boldsymbol{\rho}_{\mathrm{d}}[\mathbf{P_{25}} + 1.375\mathbf{S} + 1.8(\mathbf{OC_1} + \mathbf{OC_2}) + \mathbf{BC_1} + \mathbf{BC_2} + \mathbf{D_1} + 0.286\mathbf{D_2} + \mathbf{S_1} + 0.942\mathbf{S_2}], \quad (13)$$

where $\boldsymbol{\rho}_{\mathrm{d}}$ represents the dry air density, which is multiplied by the mixing ratios of aerosol species (in $\mu g \cdot kg^{-1}$) to convert the units to $\mu g\ m^{-3}$ for consistency with the observations.

From the perspective of the optimization of emissions, four species of emission scaling factors ($\boldsymbol{\lambda}_{\mathrm{PM2.5}}$, $\boldsymbol{\lambda}_{\mathrm{SO2}}$, $\boldsymbol{\lambda}_{\mathrm{NO}}$ and $\boldsymbol{\lambda}_{\mathrm{NH3}}$) were also considered as the state variables of the DA system. Atmospheric inorganic aerosols are not only from the primary emissions, but also from secondary processes- chemical and thermodynamic transformations from the gas-phase precursors. Therefore, not only the primary sources of $PM_{2.5}$, but also the sources of the gas-phase precursors, need to be

optimized. In this study, the sources of SO_2, NO_x and NH_3 ($\mathbf{E}_{SO2}$, $\mathbf{E}_{NO}$ and $\mathbf{E}_{NH3}$), which have a large impact on the distribution of $PM_{2.5}$, were also optimized in addition to the primary sources of $PM_{2.5}$. It is noted that for the optimization of the emission scaling factors, $\mathbf{M}_{SF}$ serves as the forecast model and the observation operator reflects the combined information of emissions (in the format of $\boldsymbol{\lambda}$ in equation (6)), the physics and chemistry processes in WRF-Chem simulations and the transformation $PM_{2.5}$ from model space to observation space (equation (13)).

The direct sources of $PM_{2.5}$ include the unspeciated primary sources of $PM_{2.5}$ $\mathbf{E}_{PM2.5}$, sulfate $\mathbf{E}_{SO4}$, nitrate $\mathbf{E}_{NO3}$, organic compounds E_{org} and elemental compounds E_{BC}; all of them are given in two modes (the nuclei and accumulation modes, represented as i and j in the subscripts respectively). The ratios between the nuclei and accumulation modes were the same as in the suggested emission process for National Emission Inventory in WRF-Chem (Freitas et al., 2011). The formula of sulfate and nitrate emissions in the model are as below:

$$\mathbf{E}_{PM2.5i}:\mathbf{E}_{PM2.5j} = 1:4, \quad (14)$$

$$\mathbf{E}_{SO4i}:\mathbf{E}_{SO4j} = 1:4, \quad (15)$$

$$\mathbf{E}_{NO3i}:\mathbf{E}_{NO3j} = 1:4, \quad (16)$$

$$\mathbf{E}_{SO4i} + \mathbf{E}_{SO4j} = a * (\mathbf{E}_{PM2.5i} + \mathbf{E}_{PM2.5j} - \mathbf{E}_{EC} - \mathbf{E}_{ORG}), \quad (17)$$

$$\mathbf{E}_{NO3i} + \mathbf{E}_{NO3j} = b * \left(\mathbf{E}_{PM2.5i} + \mathbf{E}_{PM2.5j} - \mathbf{E}_{EC} - \mathbf{E}_{ORG}\right), \quad (18)$$

where $\mathbf{E}_{EC}$ represents elemental carbon and $\mathbf{E}_{ORG}$ organic compounds, and $a = 0.074$ and $b = 0.038$ were chosen based on the internal emissions and observational data. In the DA process, the first 6 species of direct sources of emissions ($\mathbf{E}_{PM2.5i}$, $\mathbf{E}_{PM2.5j}$, $\mathbf{E}_{SO4i}$, $\mathbf{E}_{SO4j}$, $\mathbf{E}_{NO3i}$, and $\mathbf{E}_{NO3j}$), which may have larger uncertainties in heavy polluted events, were updated according to the variation of $\boldsymbol{\lambda}_{PM2.5}$. $\mathbf{E}_{PM2.5i}$ and $\mathbf{E}_{PM2.5j}$ were directly updated according to the variation in $\boldsymbol{\lambda}_{PM2.5}$. The emissions ($\mathbf{E}_{SO4i}$, $\mathbf{E}_{SO4j}$, $\mathbf{E}_{NO3i}$ and $\mathbf{E}_{NO3j}$) were also updated according to the variations in $\mathbf{E}_{PM2.5i}$ and $\mathbf{E}_{PM2.5j}$.

$\mathbf{E}_{EC}$ and $\mathbf{E}_{ORG}$ of the anthropogenic emissions were not assimilated, which is a limitation in

693 this work. Besides, emissions of dust and sea salt were not assimilated. It is true that these
694 emissions are also important for the atmosphere aerosol. The reason we did not assimilate $\mathbf{E}_{EC}$
695 and $\mathbf{E}_{ORG}$ is that only the $PM_{2.5}$ measurements are used in this DA experiment. However, the
696 sources of the aerosols (especially organic aerosols) are so complex that our knowledge of their
697 formation mechanisms is far from clear. Though it is technically possible to have all emissions
698 assimilated, with such limited observations adding more control variables would cause much more
699 uncertainties in the system which might lead to unreasonable analysis.
700
701 2.3.2 Procedure for the DA system
702 Figure 2 (b) shows the workflow of the DA system. The steps in this workflow are as
703 follows.
704 (1) The persistence forecasting operator $\mathbf{M}_{SF}$ is applied to forecast the
705 background fields of the emission scaling factors $\boldsymbol{\lambda}^{f}_{PM2.5}$, $\boldsymbol{\lambda}^{f}_{SO2}$, $\boldsymbol{\lambda}^{f}_{NO}$ and $\boldsymbol{\lambda}^{f}_{NH3}$. The
706 forecast chemical fields of P_{25}, SO_2, NO and NH_3 of the previous assimilation cycle
707 are used to create the prior emission scaling factors $\boldsymbol{\lambda}^{p}_{PM2.5}$, $\boldsymbol{\lambda}^{p}_{SO2}$, $\boldsymbol{\lambda}^{p}_{NO}$ and $\boldsymbol{\lambda}^{p}_{NH3}$.
708 The background scaling factors are then generated using equation (5).
709 (2) The ensemble members of the emissions, $\mathbf{E}^{f}_{PM2.5i}$, $\mathbf{E}^{f}_{PM2.5j}$, $\mathbf{E}^{f}_{SO2}$, $\mathbf{E}^{f}_{NO}$ and
710 $\mathbf{E}^{f}_{NH3}$, are prepared according to equation (6). The corresponding emissions of $\mathbf{E}^{f}_{SO4i}$,
711 $\mathbf{E}^{f}_{SO4j}$, $\mathbf{E}^{f}_{NO3i}$ and $\mathbf{E}^{f}_{NO3j}$ are obtained based on equations (15–18). Other inorganic
712 species of the anthropogenic emission, such as $\mathbf{E}_{EC}$ and $\mathbf{E}_{ORG}$, are not perturbed for
713 WRF-Chem. However, other anthropogenic emissions, such as $\mathbf{E}_{PM2.5}$, $\mathbf{E}_{SO4}$ and
714 $\mathbf{E}_{NO3}$, are much larger than $\mathbf{E}_{EC}$ and $\mathbf{E}_{ORG}$ in most area of China, and the ensemble
715 spreads of the aerosol concentrate largely dependent on the uncertainties of those
716 anthropogenic emissions. Besides, model errors raised from the meteorology, the
717 emission and the chemical model itself are compensated to some extent through the
718 use of multiplicative inflation. In other words, the ensemble spread of the
719 concentrations can be kept at a certain level though $\mathbf{E}_{EC}$ and $\mathbf{E}_{ORG}$, are not
720 perturbed.
721 Natural emissions, such as dust and sea salt emissions were not perturbed

explicitly when the forecast emissions were generated. However, emissions of dust and sea salt were parameterized within the GOCART model (Chin et al., 2002). Within the DA system, varying meteorology across the members implicitly perturbed dust and sea salt emissions.

(3) Forced by the changed emissions ($\mathbf{E}_{PM2.5i}$, $\mathbf{E}_{PM2.5j}$, $\mathbf{E}_{SO2}$, $\mathbf{E}_{NO}$, $\mathbf{E}_{NH3}$, $\mathbf{E}_{SO4i}$, $\mathbf{E}_{SO4j}$, $\mathbf{E}_{NO3i}$ and $\mathbf{E}_{NO3j}$ were substituted by $\mathbf{E}^{f}_{PM2.5i}$, $\mathbf{E}^{f}_{PM2.5j}$, $\mathbf{E}^{f}_{SO2}$, $\mathbf{E}^{f}_{NO}$, $\mathbf{E}^{f}_{NH3}$, $\mathbf{E}^{f}_{SO4i}$, $\mathbf{E}^{f}_{SO4j}$, $\mathbf{E}^{f}_{NO3i}$ and $\mathbf{E}^{f}_{NO3j}$; the other emissions such as $\mathbf{E}_{EC}$ and $\mathbf{E}_{ORG}$ remained unchanged), WRF-Chem is run again to forecast the chemical fields $\boldsymbol{\rho}^{f}$ with the updated chemical fields of the previous assimilation cycle as the ICs. The state variables, i.e., 15 aerosol species and four scaling factors, are then prepared.

(4) The model-simulated $PM_{2.5}$ concentration at the observation space is then calculated via equation (13). At this time, the state vector $\mathbf{x}^{f} = [\mathbf{C}^{f}, \boldsymbol{\lambda}^{f}]^{T}$ was prepared.

(5) In the assimilation step, the state variables, the concentrations of 14 defined aerosol species and a 15th unspeciated aerosol, and the four species of emission scaling factors $\boldsymbol{\lambda}^{f}_{PM2.5}$, $\boldsymbol{\lambda}^{f}_{SO2}$, $\boldsymbol{\lambda}^{f}_{NO}$ and $\boldsymbol{\lambda}^{f}_{NH3}$, were optimized through EnSRF.

(6) After the assimilation step, the optimized emissions ($\mathbf{E}^{a}_{PM2.5i}$, $\mathbf{E}^{a}_{PM2.5j}$, $\mathbf{E}^{a}_{SO2}$, $\mathbf{E}^{a}_{NO}$, $\mathbf{E}^{a}_{NH3}$, $\mathbf{E}^{a}_{SO4i}$, $\mathbf{E}^{a}_{SO4j}$, $\mathbf{E}^{a}_{NO3i}$ and $\mathbf{E}^{a}_{NO3j}$) were calculated according to equations (6, 15–18) using the optimized scaling factors ($\boldsymbol{\lambda}^{a}_{PM2.5}$, $\boldsymbol{\lambda}^{a}_{SO2}$, $\boldsymbol{\lambda}^{a}_{NO}$ and $\boldsymbol{\lambda}^{a}_{NH3}$).

3. $PM_{2.5}$ observation data and errors

Hourly averaged surface $PM_{2.5}$ observations from the Ministry of Environmental Protection of China were assimilated. There were altogether 906 national control measurement sites over China. The $PM_{2.5}$ observation sites spanned most of central and eastern China but were primarily located in urban and suburban areas. So it always happened that there were more than one observation sites in certain city, which were fall into the same model grid. Since we did not know the exact station type, We randomly selected one observation site in a city for assimilation experiment

and one for verification purposes to ensure that there was at most one assimilated measurements for one model grid. Altogether 77 stations were selected for the $PM_{2.5}$ assimilation experiment and another 77 independent stations were selected for verification. Figure 1 shows the locations of 77 measurement sites used for the $PM_{2.5}$ assimilation experiment and 77 independent sites used for forecast verification.

The observation error covariance matrix **R** in equation (9) includes contributions from measurement and representation errors. Similar to the work of Schwartz et al. (2012), the measurement error ε_0 is defined as $\varepsilon_0 = 1.5 + 0.0075 * \Pi_0$, where Π_0 denotes the observational values for $PM_{2.5}$ ($\mu g\ m^{-3}$). Thus, higher $PM_{2.5}$ values were associated with larger measurement errors. Following Elbern et al. (2007) and Pagowski et al. (2010), Schwartz et al. (2012), the representativeness error ε_r depends on the resolution of the model and the characteristics of the observation locations and is calculated as $\varepsilon_r = r\varepsilon_0\sqrt{\Delta x/\mathrm{L}}$, where r is an adjustable parameter (here, $r = 0.5$), Δx is the grid spacing (here, 40.5 km), and L is the radius of influence of an observation (here, L was set to 3 km following Elbern et al. (2007), since we do not know the station type that used in this work). The total $PM_{2.5}$ error (ε_t) is defined as $\varepsilon_t = \sqrt{{\varepsilon_0}^2 + {\varepsilon_r}^2}$. The observation errors are assumed to be uncorrelated so that **R** is a diagonal matrix.

The $PM_{2.5}$ observations were subject to quality control to ensure data reliability before DA. Considering that China has had intense pollution events, $PM_{2.5}$ values larger than 800 $\mu g\ m^{-3}$ were classified as unrealistic and were not assimilated; observations with the ensemble mean of the first guess departure exceeding 100 $\mu g\ m^{-3}$ were also omitted, following Schwartz et al. (2012). The numbers of the observations were about 17700. Among them 8 observations were discarded because they were larger than 800 $\mu g\ m^{-3}$ and 243 (around 1.5%) were discarded due to the latter reasons.

4. Experimental design

Two parallel experiments were performed to evaluate the impact of $PM_{2.5}$ DA on the

779 analyses and forecasts of aerosols over China: an assimilation experiment and a
780 control experiment. Both experiments used identical WRF-Chem settings and
781 physical parameterizations.
782
783 4.1 Spin-up ensemble forecast with perturbed Initial and boundary conditions
784 The initialization and spin-up procedures were identical to those reported by
785 Schwartz et al. (2014). The ICs and lateral boundary conditions (LBCs) for the
786 meteorological fields were provided by the National Centers for Environmental
787 Prediction Global Forecast System (GFS).
788 The initial meteorological fields were created at 0000 UTC 1 October 2014 by
789 interpolating the GFS analyses onto the model domain. The 50 ensemble members
790 were then generated by adding Gaussian random noise with a zero mean and static
791 background error covariances (Torn et al., 2006) to the temperature, water vapor,
792 velocity, geopotential height and dry surface pressure fields. The ICs of each member
793 were zero in the initial aerosol fields, representing clean conditions as described by
794 Liu et al. (2011).
795 The LBCs for the meteorological fields were then interpolated from the GFS
796 analyses from 0000 UTC 1 October 2014 to 0000 UTC 16 October 2014 and
797 perturbed similarly to the initial fields at 0000 UTC 1 October 2014. The aerosol
798 LBCs of each member for all experiments were idealized profiles embedded within
799 the WRF/Chem model.
800 Fifty-member emissions were created by adding random noise to the
801 anthropogenic emissions, same as reported by Schwartz et al. (2014),

$$\mathbf{E}_{ip}^{*}(\eta,t) = \mathbf{E}_{p}(\eta,t) + \boldsymbol{W}_{ip}\boldsymbol{\sigma}_{p}^{\mathrm{E}}(\eta,t)$$

802 where $\mathbf{E}_{ip}^{*}(\eta,t)$ is the *i*th ensemble member for the *p*th emissions variable at the
803 ηth grid point and the *t*th hour, $\mathbf{E}_{p}$ is the unperturbed emissions. The term $\boldsymbol{\sigma}_{p}^{\mathrm{E}}$ is
804 the standard deviation of all $\mathbf{E}_{p}$ values and in the horizontally adjacent points of grid
805 box η at and within 2 h of t. $\boldsymbol{W}$ is a weight that was randomly drawn from a
806 standard Gaussian distribution and varied for each ensemble member and variable but

was spatially and temporally constant. No correlations between emissions variables were considered, which was a limitation of this approach. For possible negative perturbed emissions, they were set as $\mathbf{E}_{ip}^{*}(\eta, t) = 0.001 * \mathbf{E}_{p}(\eta, t)$. This will increase the prescribed emissions more or less. However, only very few data were negative. So, this influence can be negligible.

Before the first DA cycle, a 50-member ensemble of four-day WRF-Chem forecasts was performed from 0000 UTC 1 October to 2300 UTC 4 October 2014 using the perturbed ICs at 0000 UTC 1 October 2014, the corresponding perturbed LBCs and the emissions. Then a 50-member ensemble aerosol forecasts at 0000 UTC 5 October 2014 were produced.

4.2 Assimilation experiments

Two DA experiments were performed. One was the pure assimilation of chemical ICs (hereafter expC), the others was the joint adjustment of chemical ICs and source emissions (hereafter expJ). Both DA experiments had same settings except for the emissions. They were conducted from 0000 UTC 5 October 2014 to 0000 UTC 16 October 2014. The assimilation cycle interval was 1 h.

In the first DA cycle in expJ, the first 50 ensemble chemical fields were drawn from the WRF-Chem ensemble forecasts valid at 0000 UTC 5 October 2014, as described in section 4.1. Using the ensemble aerosol forecasts, the prior emission scaling factors $\boldsymbol{\lambda}_{i,t}^{\mathrm{p}}$ at 2300 UTC 4 October 2014 were calculated. $\boldsymbol{\lambda}_{i,t}^{\mathrm{p}}$ were used directly as $\boldsymbol{\lambda}_{i,t}^{\mathrm{f}}$ for the first 5 assimilation cycles (after 5 assimilation cycles, the system has been initialized, all future scaling factors could be created using the persistence forecasting operator $\mathbf{M}_{\mathrm{SF}}$). Then, the state vector $\mathbf{x}^{\mathrm{f}} = [\mathbf{C}^{\mathrm{f}}, \boldsymbol{\lambda}^{\mathrm{f}}]^{\mathrm{T}}$ was prepared. And after that, the DA cycle started.

In expC, the first chemical fields were also drawn from the WRF-Chem ensemble forecasts valid at 0000 UTC 5 October 2014. Then, the state vector $\mathbf{x}^{\mathrm{f}} = [\mathbf{C}^{\mathrm{f}}]^{\mathrm{T}}$ was prepared and the DA cycle started.

At the WRF-Chem forecast step of the subsequent assimilation cycles for both

experiments, the ICs for the chemical variables of each member were drawn from the updated chemical fields of the previous cycle. The aerosol LBCs of each member for all experiments were idealized profiles embedded within the WRF/Chem model. As for the meteorological ensemble fields, the LBCs were prepared in advance as depicted in section 4.1; the ICs of each member of the meteorological fields were drawn from the forecast meteorological fields of the previous cycle before re-centering with the GFS analysis because we do not do meteorological analysis:

$$\boldsymbol{\pi}_{i_{\mathrm{new}}} = \boldsymbol{\pi}_i + (\boldsymbol{\pi}_{\mathrm{GFS}} - \overline{\boldsymbol{\pi}}), \quad (18)$$

where $\boldsymbol{\pi}_i$ is the *i*th member of the forecast meteorological fields of the previous cycle, $\overline{\boldsymbol{\pi}}$ is the ensemble mean of the forecast meteorological fields of the previous cycle, $\boldsymbol{\pi}_{\mathrm{GFS}}$ is the meteorological field interpolated from the GFS analyses and $\boldsymbol{\pi}_{i_{\mathrm{new}}}$ is the new meteorological field used as the IC in WRF-Chem in the next cycle.

As stated in the first paragraph in this section, the settings of expC were the same as those in expJ except for the emissions. In expJ, the ensemble anthropogenic emissions were generated by using emission scaling factors. While in expC, the ensemble anthropogenic emissions were prepared by adding random noise, as stated in 4.1.

4.3 Control experiment

The control experiment was conducted for the same period as the assimilation experiment and the simulation cycle period was 1 h, as in the assimilation experiment. The first initial chemical fields were extracted from the ensemble mean valid at 0000 UTC 5 October 2014. In the subsequent simulation process, the ICs for the chemical fields were from the previous cycle's 1-h forecast. The LBCs and ICs for the meteorological fields were updated by interpolating the GFS analyses. The emissions were the prescribed emissions $\mathbf{E}_t^{\mathrm{p}}$ without any perturbation.

5. Results

Statistics for both expJ and expC were computed using the ensemble mean prior

(background) and posterior (analysis) fields (average of the 50-member ensemble). The ensemble performances were first examined. Output from the first day of the cycling DA configurations was excluded from all verification statistics to allow the ensemble fields to ‘‘spin up’’ from the initial ensemble.

As the measurement coverage is an important factor that may determine the performance in DA, we primarily focused our attention on the results from three sub-regions with comparatively dense observational coverage (Figure 1): the Beijing–Tianjin–Hebei region (JJJ, 12 stations for assimilation and 12 stations for verification); the Yangtze River delta (YRD, 24 stations for assimilation and 24 stations for verification); and the Pearl River delta (PRD, 9 stations for assimilation and 9 stations for verification).

5.1 Ensemble performance

It is important to assess the ensemble performance for an ensemble-based DA system. In a well-calibrated system, a comparison of the prior ensemble mean root-mean-square error (RMSE) with respect to the observations should equal the prior “total spread” (square root of the sum of ensemble variance and observation error variance) (Houtekamer et al., 2005). Figure 3 shows the time series for the prior ensemble mean RMSE and the total spread for $PM_{2.5}$ aggregated over all observations in the three sub-regions for expJ. It indicates that the magnitudes of both the total spread and the RMSE were influenced by the diurnal cycle and heavy air pollution. Almost all the total spreads were smaller than the RMSE, showing an insufficient spread of $PM_{2.5}$ ensemble forecasts, which is especially evident for heavy polluted period with much larger RMSEs. For expC, the characteristics of the prior ensemble mean RMSE and the total spread for $PM_{2.5}$ were very similar to that for the joint DA experiment.

The magnitudes of the ensemble spread of the emission scaling factors of the joint DA experiment were important for emission inversion. They were very stable throughout the ~10 day experiment period, which indicates that $\mathbf{M}_{SF}$ can generate

894 stable artificial data to generate the ensemble emissions. For $\boldsymbol{\lambda}^{f}_{PM2.5}$, they ranged
895 from 0.25 to 1 in most model area. Figure 3d shows the area-averaged time series
896 extracted from the ensemble spread of $\boldsymbol{\lambda}^{f}_{PM2.5}$. It shows that the ensemble spread was
897 stably distributed around 0.5, which indicates that the uncertainty of the ensemble
898 emissions was about 50%.
899
900 5.2 Impact on aerosol ICs
901 To evaluate quantitatively the impact of the ensemble assimilation system on the ICs,
902 the mean errors (bias), RMSEs and correlation coefficient (CORR) of the assimilation
903 experiment and the control run were first analyzed. These statistics were calculated
904 against independent observations over all the analyses from 6 to 16 October 2014.
905 Table 1 shows that the bias magnitudes of the control run were 15.9 and 20.6 μg m^{-3}
906 for the YRD and the PRD, respectively, suggesting a significant overestimation of the
907 WRF-Chem aerosol mass in these two sub-regions. However, a significant
908 underestimation of the aerosol mass occurred in the JJJ region, where the model bias
909 was −18.0 μg m^{-3}. The RMSEs of the control run were 81.6, 30.6 and 31.8 μg m^{-3} for
910 the JJJ, YRD and PRD regions, respectively. After assimilation, the statistics showed
911 an apparent improvement and the magnitude of the bias and the RMSE decreased for
912 both DA experiment. For expJ, both the maximum bias and the RMSE were obtained
913 in the JJJ region, and were -10.3 and 66.9 μg m^{-3}, respectively. The CORR increased
914 from 0.79, 0.60, and 0.62 to 0.83, 0.85, and 0.80 for the JJJ, YRD and PRD,
915 respectively. The statistics of expC were very similar to those of expJ. The bias and
916 the RMSE in the JJJ region were -12.2 and 64.0 μg m^{-3}, respectively. And the CORR
917 were 0.85, 0.80, and 0.80 for the JJJ, YRD and PRD, respectively. These results
918 indicate that the initial $PM_{2.5}$ fields can be adjusted efficiently by the EnSRF.
919 It is interesting to note that expC has better RMSE and CORR than expJ but poor
920 bias in JJJ. And expC has better bias and RMSE than expJ but poor CORR in PRD.
921 Maybe small number of samples caused the uncertainties of the statics. However, the
922 differences were very small. The analysis of both experiments were very similar.
923 Then the analysis increments (i.e. $\bar{\mathbf{x}}^{a} - \bar{\mathbf{x}}^{b}$) were investigated to show the direct

impact of $PM_{2.5}$ DA. They are determined by both the observation increments and the relative magnitudes of the forecast error and the observation error, based on Equation (7). From Figure 4(a), (e) and (f), the increments of both assimilation experiments were distributed around the observations as expected. However, the impact of assimilating $PM_{2.5}$ observations was not limited to the areas where observations were located, observations information was also transported to other areas through the WRF-Chem forecast. Besides, the ensemble forecasts also partly contributed to the spatial distribution of the $PM_{2.5}$ mass. Therefore, the spatial distributions of the $PM_{2.5}$ mass in both assimilation experiments were significantly different from the control run (see Figure 4(b), (c) and(d)), which suggest that assimilation $PM_{2.5}$ observations impacts greatly on the aerosol ICs. The $PM_{2.5}$ mass magnitude of both assimilation experiments were smaller than that of the control run at the lowest model level in the YRD, the PRD and in central China. Conversely, positive differences (analysis minus control) were gained in the JJJ region and in northeast China. These indicated the reduction of the overestimation or underestimation of the WRF-Chem simulation over these regions with data assimilation.

5.3 Impact on emissions

To determine the impact of assimilating $PM_{2.5}$ observations on the chemical emissions, we analyzed the area-averaged time series extracted from the forecast emission scaling factors, the optimized emission scaling factors, the prior emissions and the optimized emissions. Figure 5 shows that $\boldsymbol{\lambda}^{\mathrm{f}}_{\mathrm{PM2.5}}$ were changed along with $\boldsymbol{\lambda}^{\mathrm{a}}_{\mathrm{PM2.5}}$. This indicates that observation information ingested from the previous observations was incorporated through the usage of the time smooth operator.

Figure 5 also shows that although the prior emissions $\mathbf{E}^{\mathrm{p}}_{\mathrm{PM2.5}}$ had no diurnal variation when the experiments were designed, the optimized $PM_{2.5}$ scaling factor, $\boldsymbol{\lambda}^{\mathrm{a}}_{\mathrm{PM2.5}}$, showed an obvious variation with time, as did the optimized unspeciated primary sources of $PM_{2.5}$, $\mathbf{E}^{\mathrm{a}}_{\mathrm{PM2.5}}$. Moreover, the values of $\boldsymbol{\lambda}^{\mathrm{a}}_{\mathrm{PM2.5}}$ were <1 at almost all times in the YRD and PRD, which resulted that the analyzed emission $\mathbf{E}^{\mathrm{a}}_{\mathrm{PM2.5}}$ were lower than the prior $PM_{2.5}$ emissions $\mathbf{E}^{\mathrm{p}}_{\mathrm{PM2.5}}$. In the YRD, the prior $\mathbf{E}^{\mathrm{p}}_{\mathrm{PM2.5}}$ was about 0.127 μg m^{-2} s^{-1} over all hours. After assimilation, the time-averaged

optimized $\mathbf{E}^{a}_{PM2.5}$ decreased to 0.107 μg m^{-2} s^{-1}, about 15.6% lower than the prior value. In the PRD, the prior $\mathbf{E}^{p}_{PM2.5}$ was about 0.10 μg m^{-2} s^{-1}. The time-averaged optimized $\mathbf{E}^{a}_{PM2.5}$ decreased to 0.066 μg·m^{-2} s^{-1}, leading to a decrease of 35.0%. However, larger values for the optimized $\mathbf{E}^{a}_{PM2.5}$ were obtained in the JJJ region in three periods, from 1600 UTC 6 October to 0000 UTC 8 October, from 1600 UTC 9 October to 0000 UTC 10 October, and from 1600 UTC 13 October to 0000 UTC 15 October as a result of the increased optimized scaling factor $\boldsymbol{\lambda}^{a}_{PM2.5}$. This may have been caused by the burning of crop residues during harvesting in this region (Li et al., 2016), which was not taken into account in the prior emissions. However, the $PM_{2.5}$ measurements network was still spatially sparse and heterogeneous in this work. Almost all measurements were located in the city and no data available in the rural. Meanwhile, the crop residues burning always occur in the rural region. Therefore, the $PM_{2.5}$ measurements network can only capture the burning information a few hours later. Hence, although the system is able to detect the emission changes caused by burning events, the time that the system started to show increased scaling factors might be not accurate enough (may shift a few hours later). Maybe a Kalman smoother would have been a better system to solve this problem.

The NO, SO_2 and NH_3 emissions were all adjusted to some extent by our DA approach (see Figure 6). The NO emissions increased by 41.3, 43.7 and 20.3% in the JJJ, YRD and PRD regions, respectively. The SO_2 emissions increased by 16.3, 10.0 and 18.3% and the NH_3 emissions increased by 16.7, 7.8 and 7.5% in the JJJ, YRD and PRD regions, respectively.

Figure 7 shows the spatial distribution of the time-averaged scaling factors $\boldsymbol{\lambda}^{a}_{PM2.5}$ at the lowest model level over all hours from 6 to 16 October 2014, since the emissions at higher levels were so small that the impact of assimilating $PM_{2.5}$ observations was negligible. Figure 8 shows the distribution of $\mathbf{E}^{p}_{PM2.5}$ and the time-averaged differences between the ensemble mean of the assimilation and the prior values.

These patterns are consistent with those in Figure 5. Negative differences were obtained in most areas of the YRD and PRD, indicating that the $PM_{2.5}$ DA primarily decreased the $PM_{2.5}$ emissions. Conversely, positive differences were obtained in

South Hebei, North Henan and Southeast Shanxi provinces, indicating that DA increased the $PM_{2.5}$ emissions.

As the economy in China has developed, the spatiotemporal distribution of emissions has changed as a result of changes in energy consumption, the structure of the energy market and advances in technology. Therefore although this inventory of emissions may have correctly described anthropogenic emissions in 2006 when it was constructed, it is not representative of the anthropogenic emissions in 2014. Theoretically, the assimilated emissions should reduce the uncertainty in the prior emissions as a result of the application of observations. Different from the situations that standard national emission inventories were reported by government in USA, European or other countries, the rapid economic development and complexity of emission sources in China lead to large uncertainties in the current emission inventories even for the latest version. Thus it's impossible for us to conduct the direct evaluation on emissions.

Although we had no direct emission observations to evaluate the analyzing emissions, which was a challenging to many emission inversion research teams (e.g. Tang et al, 2011; Miyazaki et al., 2012; Ding et al., 2015; Mclinden et al., 2016; etc.), the improvement of emissions can be verified in terms of two aspect, the diurnal variation and the location of increased emissions. The diurnal variation in the assimilated emissions verified this statement to some extent. Especially in the PRD and YRD, $\mathbf{E}^{a}_{PM2.5}$ in the daytime were always larger than those in the night, which agreed well with Olivier et al. (2003), the WRAP (2006) and Wang et al. (2010). In addition, the locations of the larger values for the optimized $E^{a}_{PM2.5}$ in the JJJ region was in good agreement with the place of the crop residues burning *traced by the* environmental satellite of China. There were 10, 231, 37 and 3 *crop residue burning spots in Hebei, Henan, Shandong and Shanxi province respectively* from 5 to 11 October 2014 and 7, 20, 5 and 21 *respectively* from 12 to 18 October 2014 (Weekly Crop Residue Burning Monitoring Report traced by Environmental Satellite, *2015a, 2015b*).

However, the analysis emissions are only a mathematical optimum. They are influenced greatly by the model errors and the observation errors. In addition, only surface $PM_{2.5}$ observations were applied in this work, which may lack abundant constraint on the sources of the secondary aerosol precursors. More observations are needed to obtain reliable emissions for the sources of the gas-phase precursors.

5.4 Verification of aerosol forecasting

For the assimilation experiment, 48-h forecasts were performed at each 0000 UTC from 6 to 16 October 2014 with the hourly forecast output for both assimilation experiments. For the verification forecasting experiment for expJ (hereafter fcJ), the ensemble mean of the analyzed ICs and emissions of expJ were used in this longer-range model forecast. For the verification forecasting experiment for expC (hereafter fcC), the ensemble mean of the analyzed ICs of expC and the prescribed anthropogenic emissions were used.

In order to get a more visualized picture of the impact of DA for both assimilation experiments, time series of the hourly $PM_{2.5}$ extracted from the analysis (AN), the control run (CT) and the hourly output of 48-h forecast (fc24 for the first day forecast and fc48 for the second day forecast) were compared with the observations (OBS) for three megacities Beijing, Shanghai and Guangzhou, respectively (Figure 9). As expected, the time series of the analysis (also the background) were consistent with the observations. The control run showed large deviations from the observations, especially in Shanghai and Guangzhou. Benefit from DA on both the first day and the second day forecasts can be clearly seen.

The bias and the RMSE of the surface $PM_{2.5}$ forecasts as a function of forecast range was then calculated against the independent observations for the three sub-regions (Figure 10). Both the bias and the RMSEs of the control run were characterized by the diurnal cycle in the YRD and PRD. The largest errors were seen at 2100 UTC in the YRD (about 29 $\mu g \cdot m^{-3}$ for bias and 37 $\mu g \cdot m^{-3}$ for RMSEs) and at 2300 UTC in the PRD (about 36 $\mu g \cdot m^{-3}$ for bias and 41 $\mu g \cdot m^{-3}$ for RMSEs), likely indicating significant systematic forecast errors at these times. From 0300 to 0900 UTC, the bias (about 1 $\mu g \cdot m^{-3}$ in the YRD and -5 $\mu g \cdot m^{-3}$ in the PRD) and the RMSE values (about 14 $\mu g \cdot m^{-3}$ in the YRD and 16 $\mu g \cdot m^{-3}$ in the PRD) were much smaller than at other times in both the YRD and PRD, showing that WRF-Chem performed well during this period. However, in the JJJ region, the bias (about -20 $\mu g \cdot m^{-3}$) and the RMSEs (about 50 $\mu g \cdot m^{-3}$) were always large as a result of a heavy pollution event.

After assimilation, both the magnitude of the bias and the RMSEs decreased sharply. Especially in in YRD and PRD, most bias ranged from -5 to 5 $\mu g \cdot m^{-3}$ and most RMSEs ranged from 11 to 14 $\mu g \cdot m^{-3}$, further indicating that DA greatly affected the ICs.

The improvements in the surface $PM_{2.5}$ forecasts by the joint adjustment of the ICs and emissions were very large in the YRD and PRD for expJ. Large reduction of the magnitude of the bias and the RMSEs due to assimilation can be seen for almost the entire 48-h forecast range. From 10- to 23-h and from 34- to 47-h, in particular, the relative reduction in RMSE was about 37.5%. However, the DA impact was much smaller for 3- to 9-h forecast ranges, which are at daytime of the first day forecast. In addition, the improvements were nearly negligible in PRD from 27- to 33-h, the daytime of the second day forecast, suggesting that the benefit gained from adjusting the ICs decreased progressively and eventually disappeared with model integration. And the performance was actually deteriorated in YRD during the same time. One of the possible reasons was that chemical model performed sufficiently well during daytime when the boundary layer was unstable and therefore the further improvement was more difficult. And there were always large errors during the night when the boundary layer was stable, so that large improvements could be obtained. The other possible reason can be attributed to the a priori constant emissions. The differences between the optimized $PM_{2.5}$ emissions and the prior emissions were comparatively small during the day, but the optimized $PM_{2.5}$ emissions were much smaller than the a prior emissions during the night. So that the control run could performed worse during the night and it could performed well during the day. Given the a priori variable emissions provided, the control run will perform better during the night. Nevertheless，attributed greatly to the large adjustment of chemical emissions, substantial improvements were still achieved from 34- to 47- h. These results revealed that joint adjustment of the ICs and emissions can improve surface $PM_{2.5}$ forecasts up to 48 h in the YRD and PRD.

As for expC, it seemed that large improvements in the surface $PM_{2.5}$ forecasts were gained through the adjustment of the ICs in PRD from 10- to 23-h and from 34-

to 47-h. Large reduction of the magnitude of the bias and the RMSEs due to assimilation can be seen during this period. The relative reduction in RMSE ranged from 25% to 37.5%. However, the forecasts deviated much from the observations for 3- to 9-h and 27- to 33-h forecast ranges. One of the reason may be that the adjustment of the ICs decreased the analysis field too much on the whole since the WRF-Chem forecast aerosol mass was systematically overestimated in PRD (see Figure 4, Figure 9f and Figure 10e). While this aerosol mass overestimation might be also due to the possibly overestimated emissions in some time periods (not all-day long) which are not corrected in the simulation. So the over-adjusted ICs compensated the unadjusted emissions in some period but also lead to the negative biases for the periods when emission is not overestimated or underestimated. The other factor was the diurnal variation. It is very clear that $PM_{2.5}$ mass gradually decreased with time from 0000 UTC to 0008 UTC and then obtained the smallest value. After that it increased with time from 0009 UTC to 0023 UTC obtained the largest value at about 0000 UTC. Both reasons led to the systematically underestimation of $PM_{2.5}$ mass of fcC from 3- to 9-h and from 27- to 33-h, though maybe the aerosol ICs were very close to the observations. Therefore, both the magnitude of the bias and the RMSEs of the fcC were larger than those of the control run. In addition, $PM_{2.5}$ forecasts of the fcC were benefit much from the diurnal variation and the adjustment of the ICs from 10- to 23-h and from 34- to 47-h. As a consequence, the magnitude of the corresponding bias and the RMSEs of the fcC were smaller than those of the control run. Similar statics characteristics were also gained in YRD. But the improvements were comparatively small from 10- to 23-h and from 34- to 47-h. However, the performance of fcJ was always better than that of the fcC for almost the entire 48-h forecast range in the PRD and YRD. This could be attributed much to the emissions since the ICs of both forecasts were very similar. In the forecast experiment of expC, the emissions were the default monthly anthropogenic emissions. While in the forecast experiment of expJ, the assimilated emissions were different much from the default monthly anthropogenic emissions (see Figure 5 and 6). Also, there was diurnal variation.

Both DA systems did not perform as well in the JJJ region as in the YRD and RRD and relatively smaller improvements were achieved in the first 24-h forecast. One possible reason for this result may be systematic errors due to chemistry mechanism in WRF-Chem. The sources of the aerosols are so complex that our knowledge of their formation mechanisms is far from clear and large uncertainties still exist in the model simulations. Chemical transport models have a tendency to underestimate PM concentrations, especially during episodes of heavy pollution (Denby et al., 2007) due to some missing reactions (Wang et al., 2014; Zhang et al., 2015, Zheng et al., 2015; Chen et al., 2016). Another reason can be attributed to the forecast meteorological fields. There were still large uncertainties, especially when boundary layer was stable and the wind speed was very small during episodes of heavy pollution. As a result, a large bias may be obtained in forecasts of heavy pollution given the ICs and emission inventories achieved from the joint assimilation. Another reason may be the sparse coverage of measurements. There were only 12 sites in the JJJ region (Figure 1) and the measurement coverage was much sparser than in the YRD or PRD.

6. Summary and Discussion

The EnSRF algorithm was extended to adjust the chemical ICs and the primary and precursor emissions to improve forecasts for surface $PM_{2.5}$. This system was applied to assimilate hourly surface $PM_{2.5}$ measurements from 5 to 16 October 2014 over China. To evaluate the effectiveness of DA, 48-h forecasts were performed using the optimized ICs and emissions, together with a control experiment without DA. Besides, the experiment of pure assimilation chemical ICs and the corresponding 48-h forecasts experiment were also performed for comparison. The results indicated that the forecasts with the optimized ICs and emissions performed much better than the control simulations. Large improvements were achieved for almost all the 48-h forecasts, particularly in the YRD and PRD. However, relatively smaller improvements were achieved in the first 24-h forecast in the JJJ region, which may be attributed to the sparse measurement coverage and the deficiencies in the model

system for forecasting heavy pollution. Comparing to the forecasts with only the optimized ICs, the forecasts with the joint adjustment were always much better for almost all the forecasts in the PRD and YRD. However, In the JJJ region, they were very similar.

There are still some limitations in this study. Firstly, we use the default monthly anthropogenic emissions as the prior emissions and no time variation was added to keep objective, since no resolution of temporal allocations at shorter but critical (e.g.,day-of-week, diurnal) scales is available. As shown in earlier work, the constant emissions will worsen the chemical forecasts (de Meij et al., 2006; Wang et al, 2009). For the joint DA system itself, it cannot benefit from the constant prior anthropogenic emissions. But the normalized RMSE in Figure 10g decreased due to the poor forecasts of control run. The control run will perform better when variable emissions within the day are allowed, especially during the night. As a result, the relative reduction in RMSE could not be so large during the night. Secondly, no correlations between emissions variables were considered when perturbing the emissions, which will lead to the reduction of the correlations between the variables. Thus, the chemical forecast will deviate from the truth to some degree. Fortunately, the perturbed emissions were only used in the initialization and spin-up experiment and expC. Therefore, there were no impacts on expJ and the control run except for expC. Thirdly, $\mathbf{E}_{EC}$ and $\mathbf{E}_{ORG}$ are not perturbed in expJ. However, as stated in Sect. 2.3.2, the ensemble spread of $\mathbf{OC_1}$ and $\mathbf{OC_2}$ can be kept at a certain level. As a result, $\mathbf{OC_1}$ and $\mathbf{OC_2}$ changed much contributed to the $PM_{2.5}$ assimilation in expJ, which suggests that the influence of not perturbing $\mathbf{E}_{EC}$ and $\mathbf{E}_{ORG}$ could be negligible. But, because of the too small magnitudes of $\mathbf{BC_1}$ and $\mathbf{BC_2}$, the differences (assimilation minus control) of $\mathbf{BC_1}$ and $\mathbf{BC_2}$ were nearly close to zero. Fourthly, the experiment (expE) where only emissions were assimilated was not included here. But it was still worth to simultaneously assimilate the chemical ICs and emission. For one thing, in expE, the chemical concentrations can be updated by the WRF-Chem model simulations with the assimilated emissions as the initial field in each DA cycle. That means that the 50-member ensemble forecasts were performed twice and it was time

consuming. For another, better concentration analysis could be obtained in expJ due to the simultaneous assimilation of ICs and emissions. While in expE, there may be larger uncertainties for the updated chemical concentrations through WRF-Chem due to the deficiency of chemistries and the uncertainties of the ICs. This will lead to larger uncertainties for the emission inversion. Also the improvement of $PM_{2.5}$ forecasts will be limited due to the comparatively poor chemical ICs.

This study represents the first step in the simultaneous optimization of chemical ICs and emissions and only surface $PM_{2.5}$ measurements were assimilated. In future work, gas-phase observations of SO_2, NO_2 and CO will be used to further improve the performance of this DA system.

References

Anderson, J.L.: An Ensemble Adjustment Kalman Filter for Data Assimilation, Mon.Weather Rev., 129, 2884–2903, 2001.

Adhikary, B., Kulkarni, S., Dallura, A., Tang, Y., Chai, T., Leung, L. R., Qian, Y., Chung, C. E., Ramanathan, V., and Carmichael, G. R.: A regional scale chemical transport modeling of Asian aerosols with data assimilation of AOD observations using optimal interpolation technique, Atmos. Environ., 42, 8600–8615, doi:10.1016/j.atmosenv.2008.08.031, 2008.

Barbu, A. L., Segers, A. J., Schaap, M., Heemink, A.W., and Builtjes, P. J. H.: A multi-component data assimilation experiment directed to sulphur dioxide and sulphate over Europe, Atmos. Environ., 43, 1622–1631, 2009.

Benedetti, A., Morcrette, J., Boucher, O., Dethof, A., Engelen, R., Fisher, M., Flentje, H., Huneeus, N., Jones, L., and Kaiser, J.: Aerosol analysis and forecast in the European Centre for Medium-Range Weather Forecasts Integrated Forecast System: 2. Data assimilation, J. Geophys. Res, 114, D13205, doi:10.1029/2008JD011115, 2009.

Bishop, C. H., Etherton, B. J., and Majumdar, S. J.: Adaptive sampling with the ensemble transform Kalman filter. Part I: Theoretical aspects, Mon. Weather Rev., 129, 420–436, 2001.

Chen, D., Liu, Z., Fast, J., and Ban, J.: Simulations of Sulfate-Nitrate-Ammonium (SNA) aerosols during the extreme haze events over Northern China in October 2014, Atmos. Chem. Phys. Discuss., doi:10.5194/acp-2016-222, in review, 2016.

Chin, M., Rood, R. B., Lin, S. J., Muller, J. F., and Thompson, A. M.: Atmospheric sulfur cycle simulated in the global model GOCART: Model description and global properties, J. Geophys. Res.-Atmos., 105, 24671–24687, 2000.

Chin, M., Ginoux, P., Kinne, S., Torres, O., Holben, B.N., Duncan, B. N., Martin, R.V., Logan, J.A., Higurashi, A., and Nakajima, J.: Tropospheric aerosol optical thickness from the GOCART model and comparisons with satellite and Sun photometer measurements, J. Atmos. Sci., 59(3), 461–483, 2002.

Collins, W. D., Rasch, P. J., Eaton, B. E., Khattatov, B. V., and J.-F. Lamarque, J.-F.:

1204 Simulating aerosols using a chemical transport model with assimilation of
1205 satellite aerosol retrievals: Methodology for INDOEX, J. Geophys. Res., 106,
1206 7313–7336, 2001.
1207 de Meij, A., Krol, M., Dentener, F., Vignati, E., Cuvelier, C., and Thunis, P.: The
1208 sensitivity of aerosol in Europe to two different emission inventories and
1209 temporal distribution of emissions, Atmos. Chem. Phys., 6, 4287-4309,
1210 doi:10.5194/acp-6-4287-2006, 2006.
1211 Dai, T., Schutgens, N.A.J., Goto, D. Shi, G.Y., Nakajima, T.: Improvement of aerosol
1212 optical properties modeling over Eastern Asia with MODIS AOD assim- ilation
1213 in a global non-hydrostatic icosahedral aerosol transport model, Environ. Pollut.,
1214 195, 319–329, 2014.
1215 Denby, B., Schaap, M., Segers, A.J., Builtjes, P.J.H., Horalek, J.: Comparison of two
1216 data assimilation methods for assessing PM10 exceedances on the European
1217 scale, Atmos. Environ., 42 (30), 7122–7134, 2007.
1218 Ding, J., van der A, R. J., Mijling, B., Levelt, P. F., and Hao, N.: NO_x emission
1219 estimates during the 2014 Youth Olympic Games in Nanjing, Atmos. Chem.
1220 Phys., 15, 9399-9412, doi:10.5194/acp-15-9399-2015, 2015.
1221 Dubovik, O., Lapyonok, T., Kaufman, Y. J., Chin, M., Ginoux, P., Kahn, R. A., and
1222 Sinyuk, A.: Retrieving global aerosol sources from satellites using inverse
1223 modeling, Atmos. Chem. Phys., 8, 209–250, doi:10.5194/acp-8-209-2008, 2008
1224 Elbern, H., Strunk, A., Schmidt, H., and Talagrand, O.: Emission rate and chemical
1225 state estimation by 4-dimensional variational inversion, Atmos. Chem. Phys., 7,
1226 3749–3769, doi:10.5194/acp- 7-3749-2007, 2007.
1227 Evensen, G.: Sequential data assimilation with a nonlinear quasi-geostrophic model
1228 using Monte Carlo methods to forecast error statistcs, J. Geophys. Res., 99(C5),
1229 10143–10162, 1994.
1230 Freitas, S. R.; Longo, K. M.; Alonso, M. F.; Pirre, M.; Marecal, V.; Grell, G.;
1231 Stockler, R.; Mello, R. F.; Sánchez Gácita, M.. PREP-CHEM-SRC 1.0: a
1232 preprocessor of trace gas and aerosol emission fields for regional and global
1233 atmospheric chemistry models. Geoscientific Model Development, v. 4, p.

419-433, 2011.

Ginoux, P., Chin, M. Tegen, I., Prospero, J. M., Holben, B., Dubovik, O., and Lin, S.-J.: Sources and distributions of dust aerosols simulated with the GOCART model, J. Geophys. Res., 106, 20,255–20,273, doi:10.1029/2000JD000053, 2001.

Grell, G., Peckham, S. E., Schmitz, R., McKeen, S. A., Frost, G., Skamarock, W. C., and Eder, B.: Fully coupled "online" chemistry within the WRF model, Atmos. Environ., 39, 6957–6975, doi:10.1016/j.atmosenv.2005.04.027, 2005.

Guenther, A., Hewitt, C. N., Erickson, D., Fall, R., Geron, C., Graedel, T., Harley, P., Klinger, L., Lerdau, M., McKay, W., Pierce, T., Scholes, B., Steinbrecher, R., Tallamraju, R., Taylor, J., and Zimmerman, P.: A global model of natural volatile organic compound emissions, J. Geophys. Res., 100, 8873–8892, doi:10.1029/94JD02950, 1995.

Guerrette, J. J. and Henze, D. K.: Development and application of the WRFPLUS-Chem online chemistry adjoint and WRFDA-Chem assimilation system, Geosci. Model Dev., 8, 1857-1876, doi:10.5194/gmd-8-1857-2015, 2015.

Hakami, A., Henze, D. K., Seinfeld, J. H., Chai, T., Tang, Y., Carmichael, G. R., and Sandu, A.: Adjoint inverse modeling of black carbon during the Asian Pacific Regional Aerosol Characterization Experiment, J. Geophys. Res.-Atmos., 110, D14301, doi:10.1029/2004JD005671, 2005.

Heemink, A.W., and Segers, A.J.: Modeling and prediction of environmental data in space and time using Kalman filtering, Stoch. Environ. Res. Risk Assess. 16 (3), 225–240, 2002.

Henze, D. K., Hakami, A., and Seinfeld, J. H.: Development of the adjoint of GEOS-Chem, Atmos. Chem. Phys., 7, 2413–2433, doi:10.5194/acp-7-2413-2007, 2007.

Henze, D. K., Seinfeld, J. H., and Shindell, D. T.: Inverse modeling and mapping US air quality influences of inorganic PM2.5 precursor emissions using the adjoint of GEOS-Chem, Atmos. Chem. Phys., 9, 5877–5903,

1264 doi:10.5194/acp-9-5877-2009, 2009.
1265 Houtekamer, P. L., Mitchell, H. L., Pellerin, G., Buehner, M., Charron, M., Spacek, L.,
1266 and Hansen, B.: Atmospheric data assimilation with an ensemble Kalman filter:
1267 Results with real observations, Mon. Weather Rev., 133, 604–620, 2005.
1268 Ide, K., Courtier, P., Ghil, M., and Lorenc, A. C.: Unified notation for data
1269 assimilation: operational, sequential and variational, J. Meteorol. Soc. Japan, 75,
1270 181–189, 1997.
1271 Jiang, Z., Liu, Z., Wang, T., Schwartz, C. S., Lin, H.-C., and Jiang, F.: Probing into
1272 the impact of 3DVAR assimilation of surface PM10 observations over China
1273 using process analysis, J. Geophys. Res. Atmos., 118, 6738–6749,
1274 doi:10.1002/jgrd.50495, 2013.
1275 Peters, W., Jacobson, A. R., Sweeney, C., Andrews, A. E., Conway, T. J., Masarie, K.,
1276 Miller, J. B., Bruhwiler, L. M. P., Petron, G., Hirsch, A. I., Worthy, D. E. J., van
1277 der Werf, G. R.,Randerson, J. T., Wennberg, P. O., Krol, M. C., Tans, P. P.: An
1278 atmospheric perspective on North American carbon dioxide exchange:
1279 CarbonTracker, P. Natl. Acad. Sci. USA, 104, 18925–18930, 2007.
1280 Kahnert, M.: Variational data analysis of aerosol species in a regional CTM:
1281 Background error covariance constraint and aerosol optical observation operators,
1282 Tellus, Ser. B, 60, 753–770, doi:10.1111/j.1600-0889.2008.00377, 2008.
1283 Kleist, D. T., Parrish, D. F., Derber, J. C., Treadon, R., Wu, W.-S., and Lord, S.:
1284 Introduction of the GSI into the NCEP global data assimilation system, Weather
1285 Forecast., 24, 1691–1705, 2009.
1286 Huneeus, N., Chevallier, F., and Boucher, O.: Estimating aerosol emissions by
1287 assimilating observed aerosol optical depth in a global aerosol model, Atmos.
1288 Chem. Phys., 12, 4585-4606, doi:10.5194/acp-12-4585-2012, 2012.
1289 Huneeus, N., Boucher, O., and Chevallier, F.: Atmospheric inversion of SO2 and
1290 primary aerosol emissions for the year 2010, Atmos. Chem. Phys., 13,
1291 6555-6573, doi:10.5194/acp-13-6555-2013, 2013.
1292 Hunt, B., Kostelich, E., and Szunyogh, I.: Efficient data assimilation for
1293 spatiotemporal chaos: a Local Ensemble Transfom Kalman Filter, Physica D,

230, 112–126, 2007.

Lee, E.-H., Ha, J.-C., Lee, S.-S., and Chun, Y.: PM10 data assimilation over South Korea to Asian dust forecasting model with the optimal interpolation method, Asia-Pacific J. Atmos. Sci., 49(1), 73–85, doi:10.1007/s13143-013-0009-y, 2013.

Li, Z., Zang, Z., Li, Q. B., Chao, Y., Chen, D., Ye, Z., Liu, Y., and Liou, K. N.: A three-dimensional variational data assimilation system for multiple aerosol species with WRF/Chem and an application to $PM_{2.5}$ prediction, Atmos. Chem. Phys., 13, 4265-4278, doi:10.5194/acp-13-4265-2013, 2013.

Li, J., Li, Y., Bo, Y., and Xie, S.: High-resolution historical emission inventories of crop residue burning in fields in China for the period 1990–2013, Atmos. Environ., 138, 152–161, 2016.

Liu, Z., Liu, Q., Lin, H. C., Schwartz, C. S., Lee, Y. H., and Wang, T.: Three-dimensional variational assimilation of MODIS aerosol optical depth: implementation and application to a dust storm over East Asia, J. Geophys. Res., 116, D23206, doi:10.1029/2011JD016159, 2011.

Liu, F., Zhang, Q., Tong, D., Zheng, B., Li, M., Huo, H., and He, K. B.: High-resolution inventory of technologies, activities, and emissions of coal-fired power plants in China from 1990 to 2010, Atmos. Chem. Phys., 15, 13299-13317, doi:10.5194/acp-15-13299-2015, 2015.

McLinden, C.A., Fioletov, V., Shephard, M.W., Krotkov, N., Li, C., Martin, R.V., Moran, M.D., and J. Joiner,: Space-based detection of missing sulfur dioxide sources of global air pollution, Nat. Geosci., 9, 496–500, doi:10.1038/ngeo2724, 2016.

Mijling, B. and van der A, R. J.: Using daily satellite observations to estimate emissions of short-lived air pollutants on a mesoscopic scale, J. Geophys. Res., 117, D17302, doi:10.1029/2012JD017817, 2012.

Miyazaki, K., Eskes, H. J., Sudo, K., Takigawa, M., van Weele, M., and Boersma, K. F.: Simultaneous assimilation of satellite NO_2, O_3, CO, and HNO_3 data for the analysis of tropospheric chemical composition and emissions, Atmos. Chem.

1324 Phys., 12, 9545– 9579, doi:10.5194/acp-12-9545-2012, 2012.
1325 Miyazaki, K., Eskes, H. J., Sudo, K., and Zhang, C.: Global lightning NOx production
1326 estimated by an assimilation of multiple satellite data sets, Atmos. Chem. Phys.,
1327 14, 3277–3305, doi:10.5194/acp-14-3277-2014, 2014.
1328 Ott, E., Hunt, B. R., Szunyogh, I., Zimin, A. V., Kostelich, E. J., et al.: Exploiting
1329 local low dimensionality of the atmospheric dynamics for efficient Kalman
1330 filtering, arXiv:physics/0203058, 24 pp., available at:
1331 http://arxiv.org/abs/physics/0203058v3/, 2002.
1332 Ott, E., Hunt, B. R., Szunyogh, I., Zimin, A. V., Kostelich, E. J., et al.: A local
1333 ensemble Kalman filter for atmospheric data assimilation, Tellus A, 56, 415–428,
1334 2004.
1335 Pagowski, M., Grell, G. A., McKeen, S. A., Peckham, S. E., and Devenyi, D.:
1336 Three-dimensional variational data assimilation of ozone and fine particulate
1337 matter observations: some results using the Weather Research and Forecasting –
1338 Chemistry model and Grid-point Statistical Interpolation, Q. J. Roy. Meteor. Soc.,
1339 136, 2013–2024, doi:10.1002/qj.700, 2010.
1340 Pagowski, M., and Grell, G. A.: Experiments with the assimilation of fine aerosols
1341 using an ensemble Kalman filter, J. Geophys. Res.-Atmos., 117, D21302,
1342 doi:10.1029/2012jd018333, 2012.
1343 Peng, Z., Zhang, M., Kou, X., Tian, X., and Ma, X.: A regional carbon data
1344 assimilation system and its preliminary evaluation in East Asia, Atmos. Chem.
1345 Phys., 15, 1087-1104, doi:10.5194/acp-15-1087-2015, 2015.
1346 Pope, C. A.: Review: Epidemiological basis for particulate air pollution health
1347 standards, Aerosol Sci. Tech., 32, 4–14, 2000.
1348 Pope, C. A., Burnett, R. T., Thun, M. J., Calle, E. E., Krewski, D., Ito, K., and
1349 Thurston, G. D.: Lung cancer, cardiopulmonary mortality, and long-term
1350 exposure to fine particulate air pollution, J. Am. Med. Assoc., 287, 1132–1141,
1351 2002.
1352 Rubin, J. I., Reid, J. S., Hansen, J. A., Anderson, J. L., Collins, N., Hoar, T. J., Hogan,
1353 T., Lynch, P., McLay, J., Reynolds, C. A., Sessions, W. R., Westphal, D. L., and

Zhang, J.: Development of the Ensemble Navy Aerosol Analysis Prediction System (ENAAPS) and its application of the Data Assimilation Research Testbed (DART) in support of aerosol forecasting, Atmos. Chem. Phys., 16, 3927-3951, doi:10.5194/acp-16-3927-2016, 2016.

Saide, P. E., Carmichael, G. R., Liu, Z., Schwartz, C. S., Lin, H. C., da Silva, A. M., and Hyer, E.: Aerosol optical depth assimilation for a size-resolved sectional model: impacts of observationally constrained, multi-wavelength and fine mode retrievals on regional scale analyses and forecasts, Atmos. Chem. Phys., 13, 10425-10444, doi:10.5194/acp-13-10425-2013, 2013.

Schwartz, C. S., Liu, Z., Lin, H. C., and McKeen, S. A.: Simultaneous three-dimensional variational assimilation of surface fine particulate matter and MODIS aerosol optical depth, J. Geophys. Res., 117, D13202, doi:10.1029/2011JD017383, 2012.

Schwartz, C. S., Liu, Z., Lin, H.-C., and Cetola, J. D.: Assimilating aerosol observations with a "hybrid" variational-ensemble data assimilation system, J. Geophys. Res. Atmos., 119, 4043–4069, doi:10.1002/2013JD020937, 2014.

Sekiyama, T. T., Tanaka, T. Y., Shimizu, A., and Miyoshi, T.: Data assimilation of CALIPSO aerosol observations, Atmos. Chem. Phys., 10, 39-49, doi:10.5194/acp-10-39-2010, 2010.

Schutgens, N. A. J., Miyoshi, T., Takemura, T., and Nakajima, T.: Sensitivity tests for an ensemble Kalman filter for aerosol assimilation, Atmos. Chem. Phys., 10, 6583-6600, doi:10.5194/acp-10-6583-2010, 2010.

Schutgens, N. A. J., Miyoshi, T., Takemura, T., and Nakajima, T.: Applying an ensemble Kalman filter to the assimilation of AERONET observations in a global aerosol transport model, Atmos. Chem. Phys., 10, 2561-2576, doi:10.5194/acp-10-2561-2010, 2010.

Schutgens, N., Nakata, M., and Nakajima, T.: Estimating Aerosol Emissions by Assimilating Remote Sensing Observations into a Global Transport Model, Remote Sensing,4, 3528-3543, 2012.

Tang, X., Zhu, J., Wang, Z. F., and Gbaguidi, A.: Improvement of ozone forecast over

Beijing based on ensemble Kalman filter with simultaneous adjustment of initial conditions and emissions, Atmos. Chem. Phys., 11, 12901–12916, doi:10.5194/acp-11-12901-2011, 2011.

Tombette, M., Mallet, V., and Sportisse, B.: PM10 data assimilation over Europe with the optimal interpolation method, Atmos. Chem. Phys., 9, 57-70, doi:10.5194/acp-9-57-2009, 2009.

Torn, R. D., Hakim, G. J., and Snyder, C.: Boundary conditions for limited-area ensemble Kalman filters, Mon. Weather Rev., 134, 2490–2502, 2006.

van Loon, M., Builtjes, P. J. H., and Segers, A. J.: Data assimilation of ozone in the atmospheric transport chemistry model LOTOS, Environ. Model. Softw., 15, 603–609, 2000.

Wang, J., Xu, X., Henze, D. K., Zeng, J., Ji, Q., Tsay, S.-C., and Huang, J.: Top-down estimate of dust emissions through integration of MODIS and MISR aerosol retrievals with the GEOS-Chem adjoint model, Geophys. Res. Lett., 39, L08802, doi:10.1029/2012GL051136, 2012.

Wang, Y. X., Zhang, Q. Q., Jiang, J. K., Zhou, W., Wang, B. Y., He, K. B., Duan, F. K., Zhang, Q., Philip, S., and Xie, Y. Y.: Enhanced sulfate formation during China's severe winter haze episode in January 2013 missing from current models, J.Geophys.Res.-Atmos., 119, 10.1002/2013JD021426, 2014

Wang, X.Y., Liang,. X.Z., Jiang, W.M., Tao, Z.N., Wang, J.X.L., Liu, H.N., Han Z.W., Liu, S.Y., Zhang, Y.Y., Grell, G.A., Peckham, S.E.: WRF-Chem simulation of East Asian air quality: Sensitivity to temporal and vertical emissions distributions, Atmospheric Environment,44(2010) 660-669

Whitaker, J. S., and Hamill, T. M.: Ensemble data assimilation without perturbed observations, Mon. Weather Rev., 130, 1913–1924, 2002.

Woo, J.H., Baek, J.M., Kim, J.W., Carmichaael, G.R., Thongboonchoo, N., Kim, S.T., An, J.H.: Development of a Multi-Resolution Emission Inventory and Its Impact on Sulfur Distribution for Northeast Asia, Water, Air, and Soil Pollution 148: 259–278, 2003.

Weekly Crop Residue Burning Monitoring Report ,

http://hjj.mep.gov.cn/jgjs/201510/P020151012746205487305.pdf, 2015a (in Chinese).

Weekly Crop Residue Burning Monitoring Report, http://hjj.mep.gov.cn/jgjs/201510/P020151019568921489639.pdf, 2015b(in Chinese).

Xia Y., Zhao, Y., Nielsen, C.P., Benefits of China's efforts in gaseous pollutant control indicated by the bottom-up emissions and satellite observations 2000-2014, Atmospheric Environment, 136, 43-53, 2016

Yu, H., Dickinson, R. E., Chin, M., Kaufman, Y. J., Geogdzhayev, B., and Mishchenko, M. I.: Annual cycle of global distributions of aerosol optical depth from integration of MODIS retrievals and GOCART model simulations, J. Geophys. Res., 108(D3), 4128, doi:10.1029/2002JD002717, 2003.

Yumimoto, K., Uno, I., Sugimoto, N., Shimizu, A., and Satake, S.: Adjoint inverse modeling of dust emission and transport over East Asia, Geophys. Res. Lett., 34, L00806, doi:10.029/2006GL028551, 2007.

Yumimoto, K., Uno, I., Sugimoto, N., Shimizu, A., Liu, Z., and Winker, D. M.: Adjoint inversion modeling of Asian dust emission using lidar observations, Atmos. Chem. Phys., 8, 2869-2884, doi:10.5194/acp-8-2869-2008, 2008.

Yumimoto, K., Nagao, T.M., Kikuchi, M., Sekiyama, T.T, Murakami, H.,Tanaka, T.Y., Ogi, A., Irie, H., Khatri, P., Okumura, H., Arai, K., Morino, I., Uchino, O., Maki, T.: Aerosol data assimilation using data from Himawari-8, a next-generation geostationary meteorological satellite, Geophys. Res. Lett., 43, 5886–5894, 2016.

Yin, X.M., Dai, T., Xin, J.Y., Gong, D.Y., Yang, J., Teruyuki, N., Shi, G.Y.: Estimation of aerosol properties over the Chinese desert region with MODIS AOD assimilation in a global model, Adv. Clim. Change Res., 7, 90–98, 2016.

Zhang, J., Reid, J. S., Westphal, D., Baker, N., and Hyer, E.: A System for Operational Aerosol Optical Depth Data Assimilation over Global Oceans, J. Geophys. Res., 113, D10208, doi:10.1029/2007JD009065, 2008.

Zhang, Q., Streets, D. G., Carmichael, G. R., He, K. B., Huo, H., Kannari, A.,

Klimont, Z., Park, I. S., Reddy, S., Fu, J. S., Chen, D., Duan, L., Lei, Y., Wang, L. T., and Yao, Z. L.: Asian emissions in 2006 for the NASA INTEX-B mission, Atmos. Chem. Phys., 9, 5131-5153, doi:10.5194/acp-9-5131-2009, 2009.

Zhang, L., Liu, L. C., Zhao, Y. H., Gong, S. L., Zhang, X. Y., Henze, D. K., Capps, S. L., Fu, T. M., Zhang, Q., and Wang, Y. X.: Source attribution of particulate matter pollution over North China with the adjoint method, Environ.Res.Lett., 10, Artn 08401110.1088/1748-9326/10/8/084011, 2015.

Zheng, B., Zhang, Q., Zhang, Y., He, K. B., Wang, K., Zheng, G. J., Duan, F. K., Ma, Y. L., and Kimoto, T.: Heterogeneous chemistry: a mechanism missing in current models to explain secondary inorganic aerosol formation during the January 2013 haze episode in North China, Atmos.Chem.Phys., 15, 2031-2049, 10.5194/acp-15-2031-2015, 2015.

List of Figures and Table

Figure 1. Locations of 77 PM2.5 assimilation observation stations (black dot) and the 77 independent observation stations (red triangle) in the model domain. The three colored boxes mark sub-regions with relatively dense coverage for the Beijing–Tianjin–Hebei region (JJJ, 12 assimilation stations and 12 independent stations, red box), the Yangtze River delta (YRD, 24 assimilation stations and 24 independent stations, blue box) and the Pearl River delta (PRD, 9 stations and 9 independent stations, green box).

Figure 2. (a) Framework of M_{SF} and (b) flow chart of the data assimilation system that simultaneously optimizes the chemical initial conditions and emissions.

Figure 3. Time series of prior ensemble mean RMSE and total spread for PM2.5 concentrations aggregated over all observations over the three sub-regions: (a) Beijing–Tianjin–Hebei region; (b) Yangtze River delta; (c) Pearl River delta; and (d) time series of the area mean ensemble spread for $\lambda_{PM2.5}$ over the three sub-regions.

Table 1. Comparison of the surface PM2.5 mass concentrations from the control and assimilation experiments to observations over all analysis times from 6 to 16 October 2014.

Figure 4. Spatial distribution of the PM2.5 mass (μg·m−3) of the (a) observations; (b) simulation of the control run; (c) analysis of expJ; (d) analysis of expC; (e) increments of expJ; (f) increments of expC; at the lowest model level averaged over all hours from 6 to 16 October 2014.

Figure 5. Hourly area-averaged time series of emission scaling factors (black) extracted from the ensemble mean of the analyzed $\lambda^{a}_{PM2.5}$ and the corresponding analyzed unspeciated primary PM2.5 emissions $E^{a}_{PM2.5}$ (blue) over the three sub-regions: (a) Beijing–Tianjin–Hebei region; (b) Yangtze River delta; and (c) Pearl River delta.

Figure 6. Hourly area-averaged time series of emission scaling factors extracted from the ensemble mean of the analyzed (a) $\boldsymbol{\lambda}^{a}_{NO}$; (a) $\boldsymbol{\lambda}^{a}_{SO2}$; (a) $\boldsymbol{\lambda}^{a}_{NH3}$ over the three sub-regions: Beijing–Tianjin–Hebei region (JJJ, black), Yangtze River delta (YRD, green), and Pearl River delta (PRD, blue).

Figure 7. Spatial distribution of $\lambda_{PM2.5}$ at the lowest model level averaged over all hours from 6 to 16 October 2014.

Figure 8. Spatial distribution of (a) the prior unspeciated primary sources of PM2.5 (μg·m−2 s−1) and (b) the time-averaged differences between the ensemble mean analysis and the prior values (μg· m−2 s−1) at the lowest model level averaged over all hours from 6 to 16 October 2014.

Figure 9. Time series of the hourly PM2.5 obtained from observations (circle), analysis (blue line), control run (black line) and hourly output of 48-h forecast in three megacities: (a) Beijing; (c) Shanghai; and (e) Guangzhou in expJ and (b) Beijing; (d) Shanghai; and (f) Guangzhou in expC. See text in section 5.4.

Figure 10. Bias of surface PM2.5 as a function of forecast range calculated against independent observations over the three sub-regions: (a) Beijing–Tianjin–Hebei region; (c) Yangtze River delta; (e) Pearl River delta and RMSE over (b) Beijing–Tianjin–Hebei region; (d) Yangtze River delta; (f) Pearl River delta; (g) Normalized RMSE (assimilation divided by control) for expJ and (h) (g) Normalized RMSE for expC.

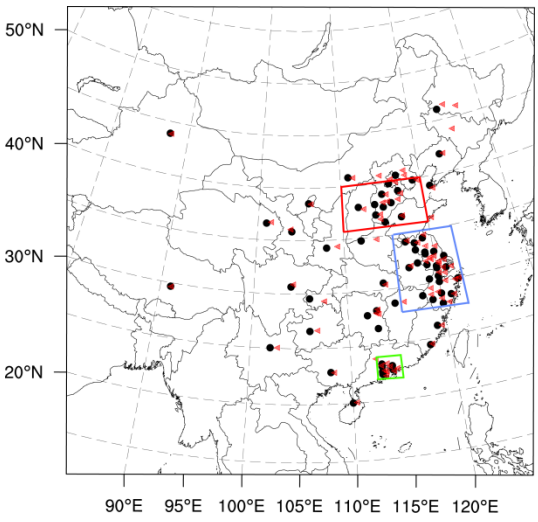

Figure 1. Locations of 77 $PM_{2.5}$ assimilation observation stations (black dot) and the 77 independent observation stations (red triangle) in the model domain. The three colored boxes mark sub-regions with relatively dense coverage for the Beijing–Tianjin–Hebei region (JJJ, 12 assimilation stations and 12 independent stations, red box), the Yangtze River delta (YRD, 24 assimilation stations and 24 independent stations, blue box) and the Pearl River delta (PRD, 9 stations and 9 independent stations, green box).

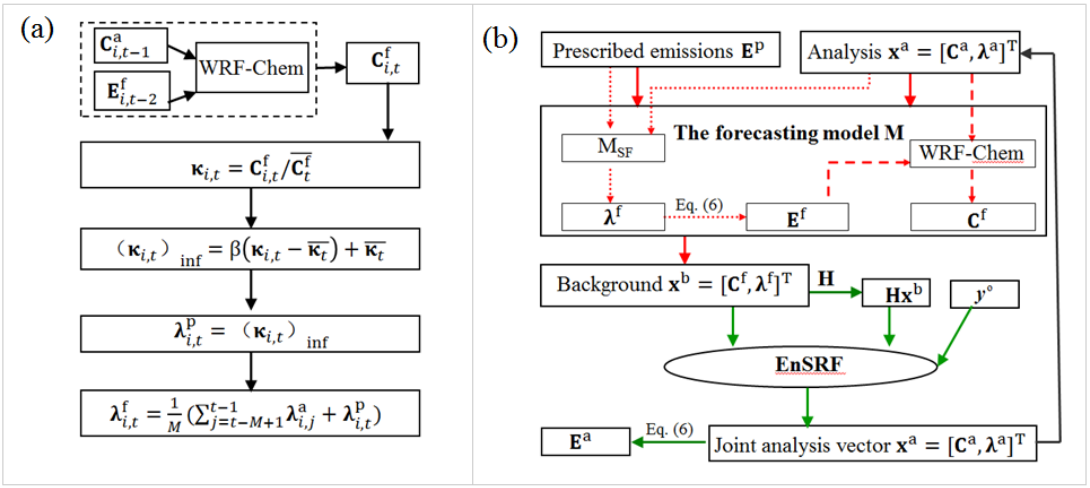

Figure 2. (a) Framework of $\mathbf{M}_{SF}$ and (b) flow chart of the data assimilation system that simultaneously optimizes the chemical initial conditions and emissions.

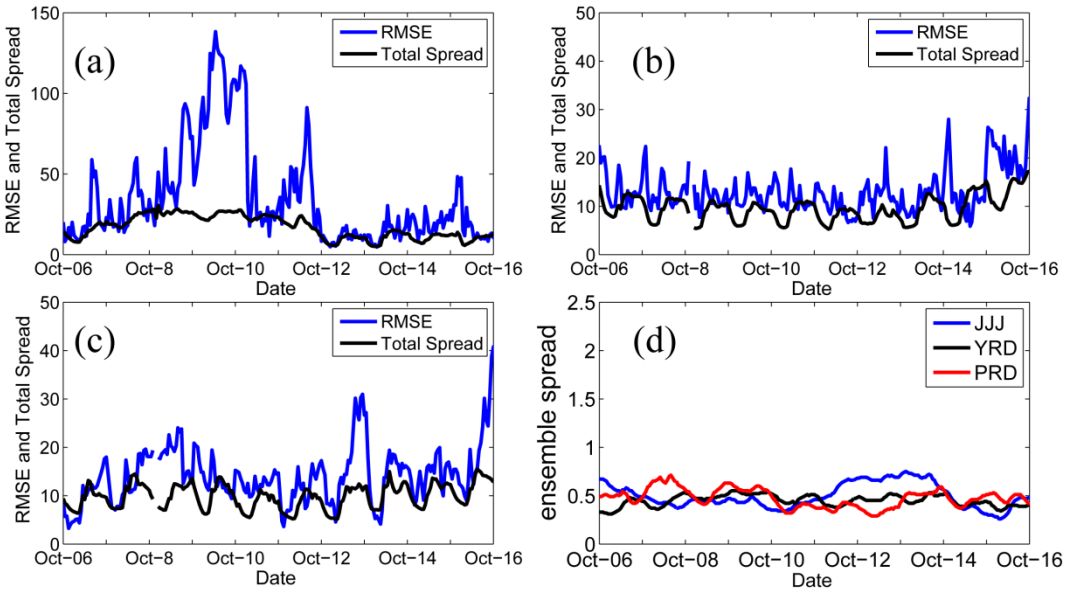

Figure 3. Time series of prior ensemble mean RMSE and total spread for $PM_{2.5}$ concentrations aggregated over all observations over the three sub-regions: (a) Beijing–Tianjin–Hebei region; (b) Yangtze River delta; (c) Pearl River delta; and (d) time series of the area mean ensemble spread for $\boldsymbol{\lambda}_{PM2.5}$ over the three sub-regions.

Table 1. Comparison of the surface $PM_{2.5}$ mass concentrations from the control and assimilation experiments to observations over all analysis times from 6 to 16 October 2014.

Region	Experiment	Mean observed value	Mean simulated value	BIAS	RMSE	CORR
Beijing–Tianjin–Hebei	Control	116.3	98.3	−18.0	81.6	0.790
	expJ		106.0	−10.3	66.9	0.827
	expC		104.1	-12.2	64.0	0.845
Yangtze River delta	Control	48.5	64.4	15.9	30.6	0.593
	expJ		46.9	-1.6	15.3	0.846
	expC		46.1	-2.4	17.3	0.803
Pearl River delta	Control	61.8	82.4	20.6	31.8	0.624
	expJ		66.5	4.7	16.1	0.800
	expC		64.1	-2.3	15.6	0.797

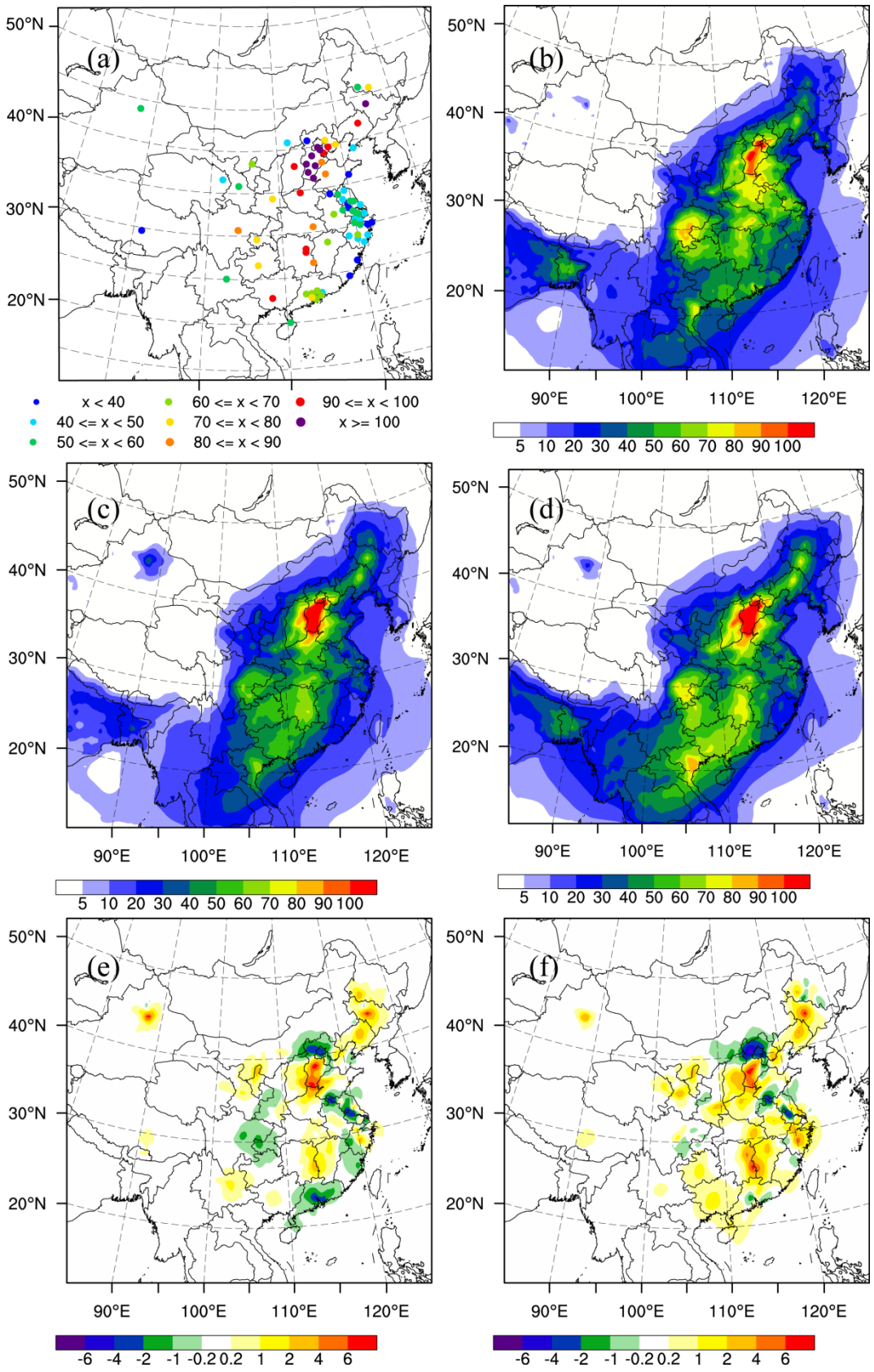

Figure 4. Spatial distribution of the $PM_{2.5}$ mass (μg m^{-3}) of the (a) observations; (b) simulation of the control run; (c) analysis of expJ; (d) analysis of expC; (e) increments of expJ; (f) increments of expC; at the lowest model level averaged over all hours

from 6 to 16 October 2014.

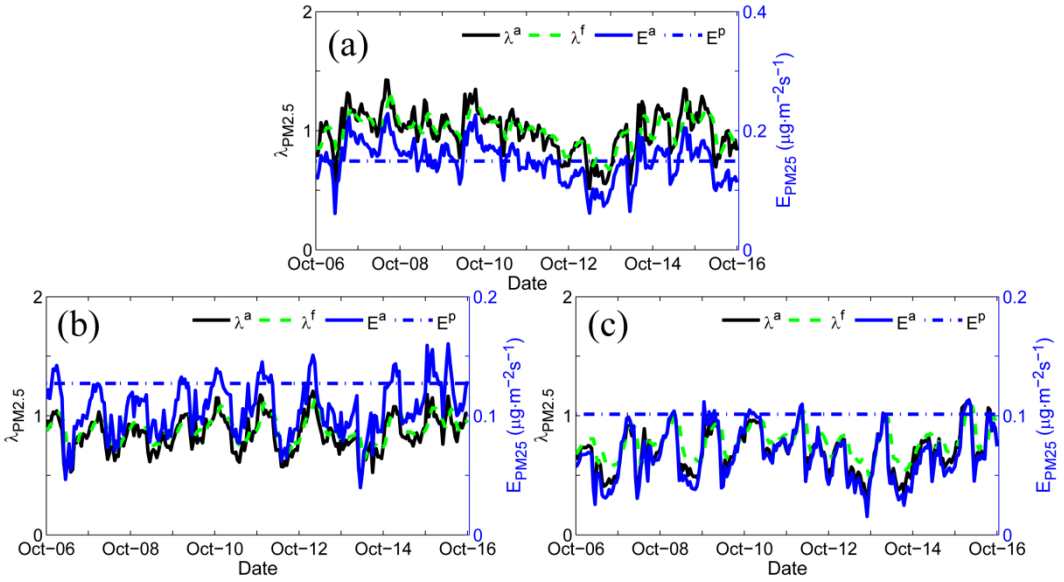

Figure 5. Hourly area-averaged time series of emission scaling factors (black) extracted from the ensemble mean of the analyzed $\boldsymbol{\lambda}^{a}_{PM2.5}$ and the corresponding analyzed unspeciated primary $PM_{2.5}$ emissions $\mathbf{E}^{a}_{PM2.5}$ (blue) over the three sub-regions: (a) Beijing–Tianjin–Hebei region; (b) Yangtze River delta; and (c) Pearl River delta.

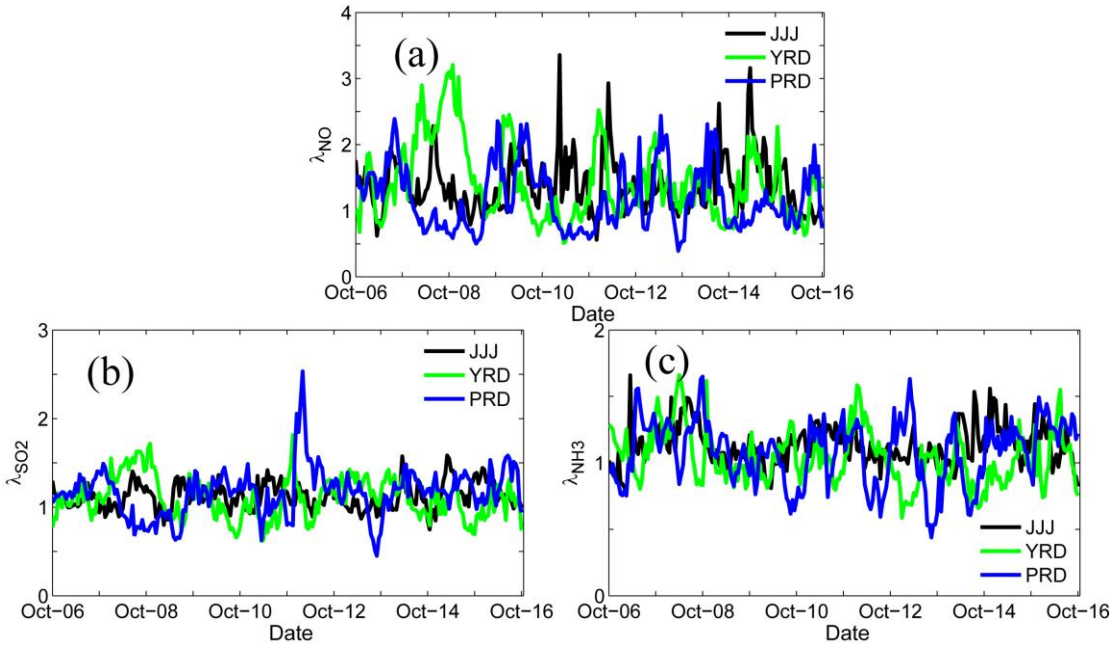

Figure 6. Hourly area-averaged time series of emission scaling factors extracted from the ensemble mean of the analyzed (a) $\boldsymbol{\lambda}^{a}_{NO}$; (a) $\boldsymbol{\lambda}^{a}_{SO2}$; (a) $\boldsymbol{\lambda}^{a}_{NH3}$ over the three sub-regions: Beijing–Tianjin–Hebei region (JJJ, black), Yangtze River delta (YRD, green), and Pearl River delta (PRD, blue).

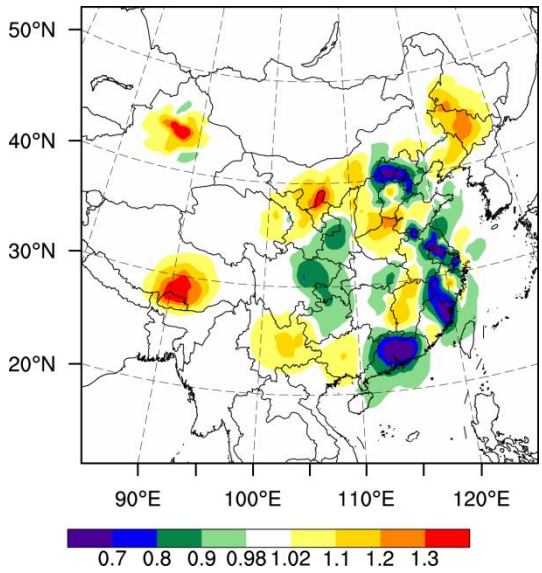

Figure 7. Spatial distribution of $\boldsymbol{\lambda}_{\mathrm{PM2.5}}$ at the lowest model level averaged over all hours from 6 to 16 October 2014.

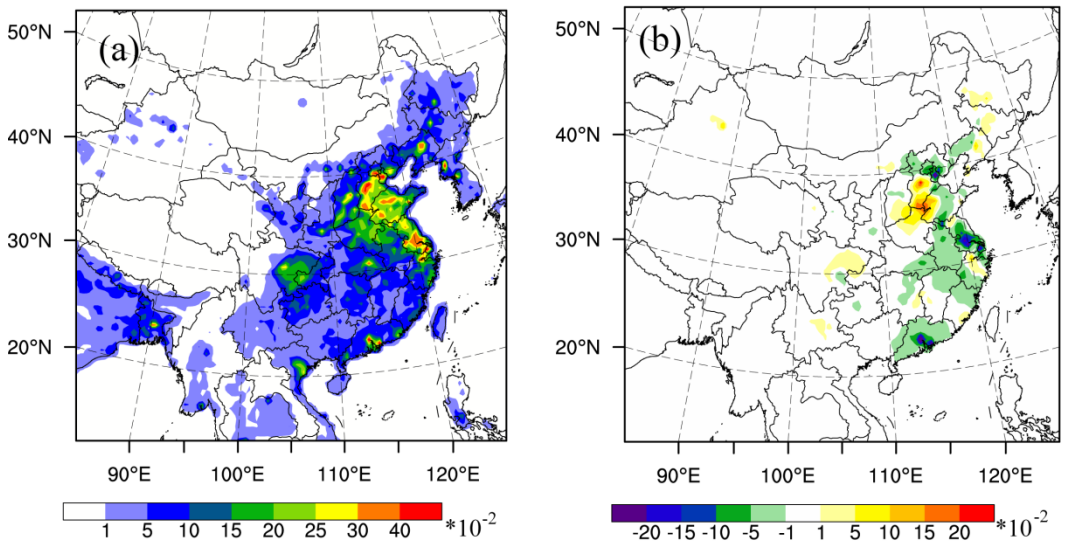

Figure 8. Spatial distribution of (a) the prior unspeciated primary sources of $PM_{2.5}$ ($\mu g\ m^{-2}\ s^{-1}$) and (b) the time-averaged differences between the ensemble mean analysis and the prior values ($\mu g \cdot m^{-2}\ s^{-1}$) at the lowest model level averaged over all hours from 6 to 16 October 2014.

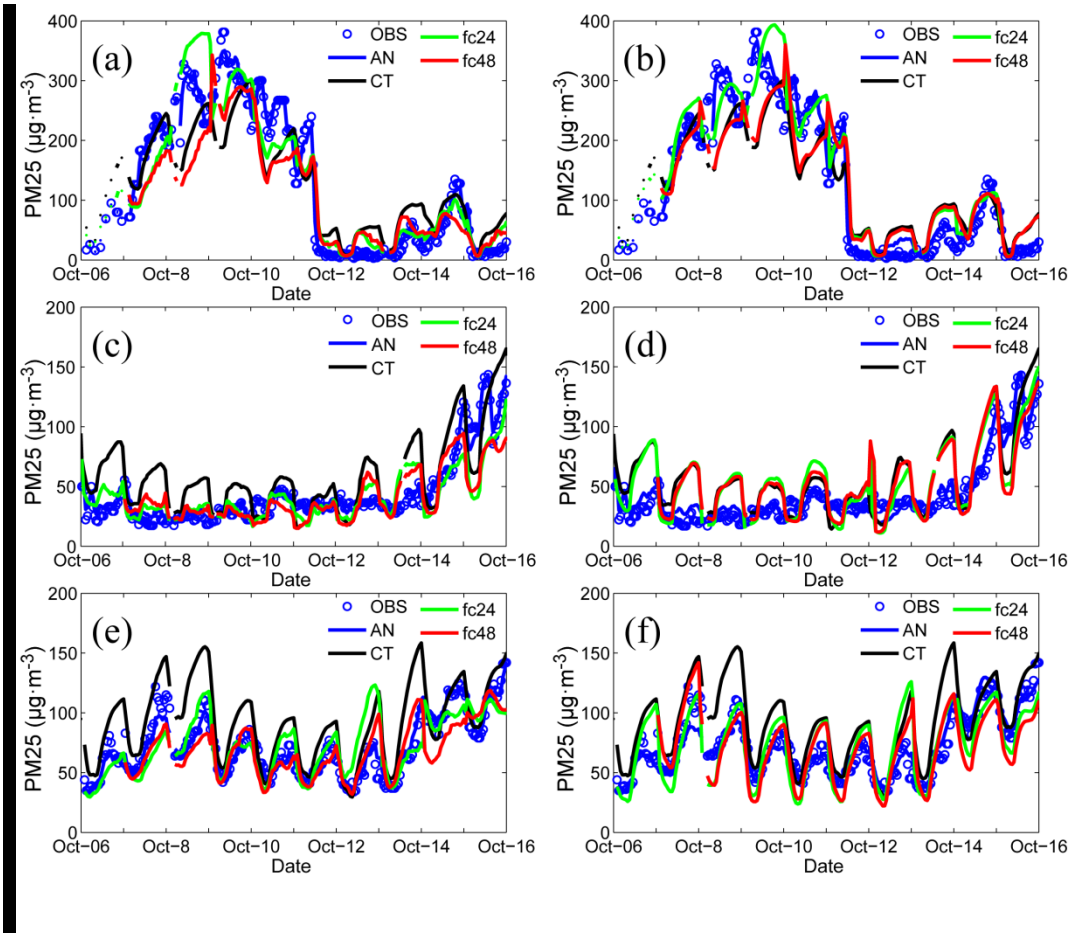

Figure 9. Time series of the hourly $PM_{2.5}$ obtained from observations (circle), analysis (blue line), control run (black line) and hourly output of 48-h forecast in three megacities: (a) Beijing; (c) Shanghai; and (e) Guangzhou in expJ and (b) Beijing; (d) Shanghai; and (f) Guangzhou in expC. See text in section 5.4.

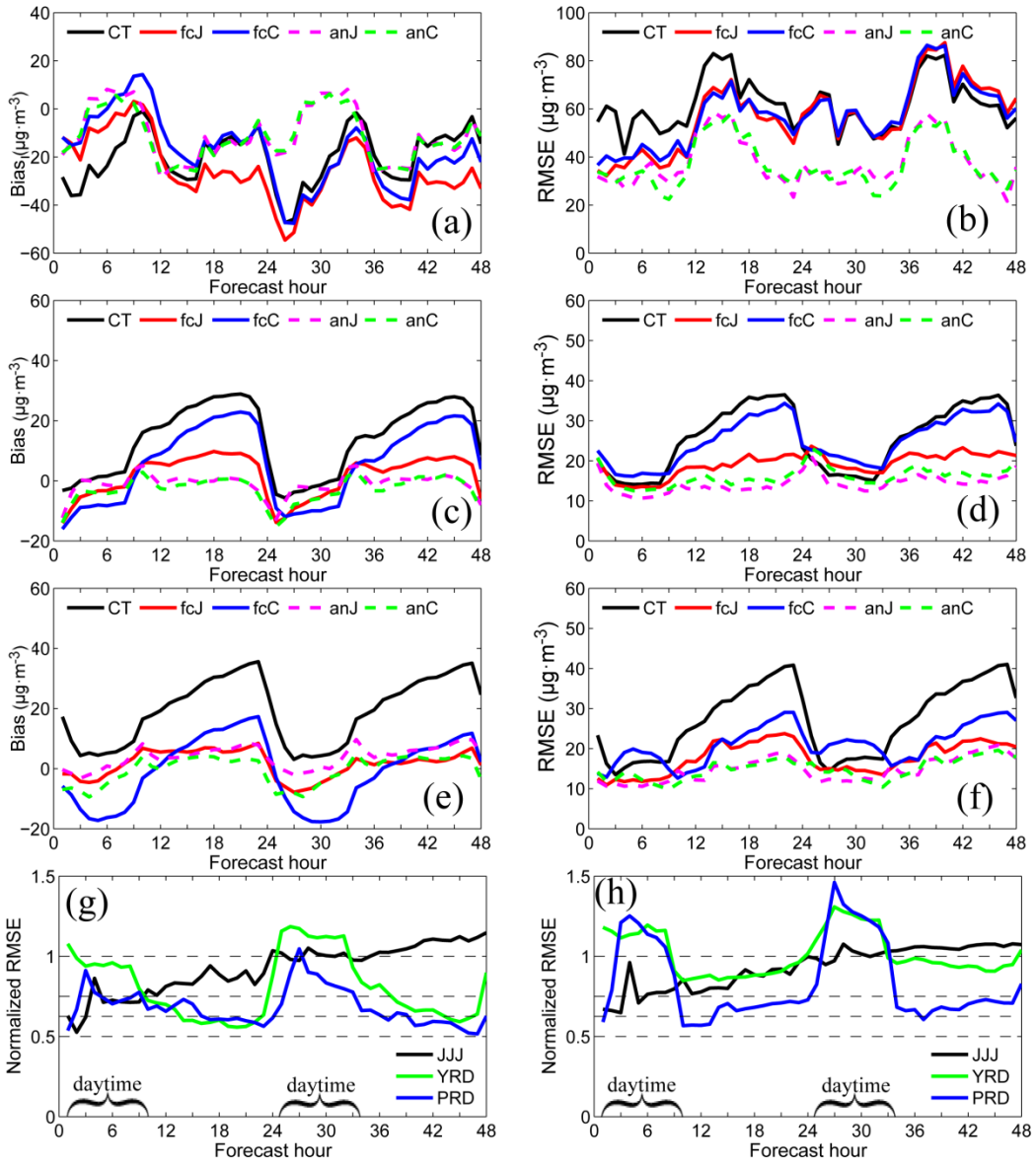

Figure 10. Bias of surface $PM_{2.5}$ as a function of forecast range calculated against all the independent observations over the three sub-regions shown in figure 1: (a) Beijing–Tianjin–Hebei region; (c) Yangtze River delta; (e) Pearl River delta and RMSE over (b) Beijing–Tianjin–Hebei region; (d) Yangtze River delta; (f) Pearl River delta; (g) Normalized RMSE (assimilation divided by control) for expJ and (h) (g) Normalized RMSE for expC. The statistics were computed from 6 to 16 October.